

Applying of zero residue level concept in integrated management of toxic and solid wastes as a sustainable approach

Anaheed Saad Hameed¹ , Alanood A. Alsarayreh² , Mohammed Nsaif Abbas^{3*} 

¹ Environmental Engineering Department, College of Engineering, Mustansiriyah University, Baghdad, Iraq

² Chemical Engineering Department, College of Engineering, Mutah University, Al Karak, Jordan

³ Materials Engineering Department, College of Engineering, Mustansiriyah University, Baghdad, Iraq

* Corresponding author's e-mail: mohammed.nsaif.abbas@uomustansiriyah.edu.iq

ABSTRACT

This study aims to explore a dual-purpose approach for environmental and construction challenges by investigating the adsorption of Iron (III) from produced water using almond shells. Also, it seeks to provide an innovative solution by evaluating the potential of the adsorbent and its subsequent use as a sustainable additive in concrete. Employing simulating contaminated solutions, the operating parameters studied were iron concentration, pH, agitation speed, initial iron ion concentration, almond shell dose, treatment time and temperature. The obtained outcomes exhibited that the highest adsorption capacity and the iron recovery from aqueous solutions were 20.376 mg·g⁻¹ and 96.52%, respectively. The results also indicated that the process obeyed the Langmuir and the intra-particle diffusion models with a correlation coefficient of 0.9999, according to the isothermal and kinetic studies, respectively. Thermodynamically, the adsorption was favorable randomness, endothermic and spontaneous, and was of the chemical type according to the enthalpy value. FTIR examination showed that the almond shells before adsorption possessed a number of functional groups, while the SEM test showed that the adsorption medium suffered significant changes as a result of treatment with solutions contaminated with iron. The surface area of virgin almond shells was 7.7 m²·g⁻¹ and adsorption led to the accumulation of iron ions and reduced this area to less than 0.75 m²·g⁻¹ after the end of treatment. The remnant Fe⁺³-almond shells was tested to use as a reinforcing material for concrete mixture of (4:2:1). The results showed that 2.8 wt.% was the best ratio and the compressive strength increased by more than 206% and 195% for the 7- and 28-days tested concrete cubes, respectively.

Keywords: produced water, iron (III) ions, batch adsorption, reinforcing material, concrete, and agro-waste.

INTRODUCTION

The term “produced water” refers to the water that is generated as a by-product during the extraction process of oil and natural gas, accompanying these resources as they are brought to the surface (Alhamd et al., 2024a). Typically, oil wells yield significant volumes of produced water, whereas natural gas wells produce water with lower oil content (Adnan et al., 2023). The quantity and quality of produced water varies from one country to another, and from one oil field to another, depending on the geological parameters, the type of field, and the ages of the wells. Its amount can range between 3–10 times the quantity of oil and gas extracted (Rajbongshi and

Gogoi, 2024). Globally, the produced water associated with oil extraction from the ground is produced in huge quantities, reaching to 11 billion liters of water per day according to the lowest estimates. Thus, this huge amount of produced water can be an important source for many different uses, at least in areas adjacent to oil fields (Alhamd et al., 2024c). However, this large water source is often contaminated with various types of pollutants and requires multiple treatments to make it suitable for agricultural or industrial uses or even for human consumption (Abdulhammed and Alhamd, 2024). Produced water pollutants include different types such as hydrocarbons, dissolved salts, silts, and organic compounds. The most important types of pollutants are various

heavy metals, especially iron (Jiménez et al., 2018). According to the standards of the WHO, the US Environmental Protection Agency (USEPA) and the Iraqi standard specification, the iron ion concentration in drinking water should not exceed 0.3 ppm (Khaleel et al., 2022). Although in normal doses it is non-toxic, the presence of iron ions in water can enhance the occurrence of complex chemical reactions (Ibrahim et al., 2020a) that lead to the formation of mineral deposits that may affect the quality of water and hinder its use in the future, in addition to its multiple adverse impacts on humans and other living organisms, the environment, and industry (Zhang et al., 2023). High concentrations of this heavy metal affect internal organs over time, as well as digestive problems such as nausea and vomiting (Ali and Abbas, 2020). Some people suffer from hemochromatosis, a condition that causes iron to build up in vital organs such as the liver and heart, which can lead to serious health problems (Porter and Rawla, 2024). In aquatic environments, high concentrations of iron cause the death of marine organisms such as fish, as iron reduces the levels of dissolved oxygen in the water, which harms organisms that depend on aquatic respiration (Bakker et al., 2016). These high concentrations can slow plant growth or cause negative changes in their ability to absorb nutrients from the soil, thus affecting agricultural production (Ning et al., 2023). Environmentally, the infiltration of contaminated water with iron ions into soil or water bodies can lead to long-term effects, such as contamination of groundwater and surface water sources (Abbas and Abbas, 2013a). When iron accumulates in waterways, it can cause iron precipitates to form on the bottom of water bodies, blocking light and affecting the photosynthesis of aquatic plants, leading to an imbalance in the environment (Ibrahim et al., 2020b). Conversely, the presence of iron ions in industrial water can cause corrosion in pipes and metal equipment, leading to higher maintenance and repair costs (Nguyen and Tadi, 2024). This is a major problem in industrial facilities and power plants that use large amounts of water. Consequently, eliminating heavy metal ions from polluted water is important to ensure environmental and human health safety, and to maintain the efficiency of industrial processes (Ejaz et al., 2023). Numerous manners are employed to treat water polluted with heavy metals such as adsorption, advanced oxidation processes (AOPs), chemical precipitation,

membrane filtration, electrocoagulation, flotation, ion exchange, bioremediation, phytoremediation, chemical reduction, electro dialysis, coagulation and flocculation, ozonation, bio-membrane filtration, chemical fixation, photocatalysis, evaporation, thermal desorption and others (Abbas et al., 2020). Although many technologies for treating water contaminated with heavy metals are effective, they have disadvantages and drawbacks. Some methods are very expensive and require high energy, regular maintenance, or large areas, making them unsuitable for developing countries or small projects. Other methods produce large amounts of sediment and waste that require additional treatment, while other methods' equipment is affected by corrosion resulting from the treatment process (Bayuo et al., 2023). In addition, the long treatment times of many of the technologies used may make them an unsuitable option for treating contaminated water. Finally, some methods may cause unexpected environmental impacts that require time, effort, and cost to eliminate. In contrast, adsorption technology stands out among all the previous methods as one of the touching and favorable techniques for treating contaminated aqueous solutions (Abbas et al., 2019a). This technology is characterized by its efficiency, simplicity, and low operating costs. In addition, it does not require primary treatments, special equipment, or large areas, and at the same time does not consume a high amount of energy (Alalwan et al., 2018). Adsorption technology has proven its ability to treat water at extreme concentrations, both high and low, and also its ability to deal with several kinds of contaminants such as heavy metals (Rajaa et al., 2023), dyes (Alalwan et al., 2021), inorganic toxins (Alalwan et al., 2019), organic acids (Abbas and Abbas, 2014), pesticides (Ali et al., 2018), eutrophication elements (Abbas, 2015), water hardness (Ibrahim et al., 2021), sulfates (Abbas and Alalwan, 2019) and other soil pollutants (Abbas et al., 2021), crude petroleum contaminants (Ali et al., 2021), and purifying oil fractions (Abbas and Ibrahim, 2020). Some of the most well-known adsorption media that have contributed to proving the worth of this technology are activated carbon (Maddodi et al., 2020), zeolite (Khudair et al., 2024), alumina (Shadhan et al., 2024), and nanomaterials (Hameed and Abbas, 2024). These media are characterized by their effectiveness and ability to treat polluted environments attributable to their distinctive characteristics, including a

large surface area, diverse functional groups spread on their surface, in addition to their strong structural composition (Alhamd et al., 2024d). Nonetheless, the high production cost, the need for continuous regeneration, and the mass loss during each regeneration cycle have posed significant challenges to their broader application in processing (Ukhurebor et al., 2024). These issues prompted researchers to seek for non-expensive alternatives, and this is what agricultural and industrial waste has achieved, which represents a sustainable source, available in large quantities almost at all times and places, with a low cost, appropriate effectiveness, and negligible toxicity, and at the same time it is considered one of the effective ways to get rid of this waste (Abbas and Abbas, 2013b). Banana peels (Abdullah et al., 2023), lemon peels (Al-Hermizy et al., 2022), mandarin peels (Alhamd et al., 2024b), orange peels (Hasan et al., 2021), watermelon peels (Abbas and Nussrat, 2020), eggshells (Ali et al., 2020b), waste tea leaves (Al-Ali et al., 2023), tree leaves (Ali et al., 2024a), algae (Abbas et al., 2019b), water hyacinth (Hashem et al., 2021), aluminum foil (Ghulam et al., 2020), sunflower seed shells (Abdulkareem et al., 2023), rice husks (Abbas and Abbas, 2013c), pomegranate peels (Ali et al., 2024b), etc. showed clear ability and suitable efficiency in removing various types of pollutants at a low cost that cannot be compared with the well-known adsorption media. Nevertheless, the buildup of residues from these materials after the adsorption process, which are often toxic, remains a significant challenge. This issue has been difficult to address due to the high financial cost and the substantial efforts needed to develop an effective method for disposing of these accumulated materials (Alwan et al., 2021). The concept of zero residue level (ZRL) provides a sustainable solution to this issue, transforming these materials from undesirable waste into valuable raw materials that can be used in a cost-effective and environmentally responsible manner (Abd Ali et al., 2024). For example, rice husks loaded with lead (Abbas et al., 2022a) residues and residues of tea leaves loaded with copper have been transformed into additives to enhance the compressibility of concrete. Rice husks loaded with some heavy metals have been transformed into activated bioethanol (Hamdi et al., 2024), while pesticide residues have been utilized as rodenticide (Al-Latif et al., 2023). Other successful ways are producing acetone (Abbas et al., 2022b), and

nanoparticles (Alminshid et al., 2021), from these wastes. From this standpoint, and as it represents one of the agricultural wastes that are disposed of in large quantities annually, the purpose of this investigation is to determine the possibility of benefiting from almond shells as one of the available and low-cost agricultural wastes in removing iron (III) from the oilfield produced water accompanying the extraction of crude oil by the adsorption method, within a batch unit and under various designing parameters. Next, investigate the potential of utilizing the remaining waste as an additive to improve the compressive strength of the concrete mixture, applying the sustainability approach by achieving zero residue level (ZRL) concept.

METHODOLOGY

Real produced water

Several samples of real produced water were collected from Al-Ahdab oil field, located 180 km southeast of Baghdad, and the collection process was conducted following the procedure outlined by (Alhamd et al., 2024a). Using clean and sterile 1000 ml flasks, the samples were obtained by immersing them in the collecting pond of the produced water separated from the crude oil, then they were tightly closed and covered with a layer of aluminum foil to protect them from light. Finally, the sample labeled by number and date. The samples were transferred as quickly as possible to the laboratory to conduct the necessary physical and chemical tests and determine their components and specifications. Table 1 shows the physical properties, while Table 2 shows the chemical specifications. Table 3 and 4 show the composition of the produced water samples.

Chemicals

Many chemicals were used in this study to achieve the desired objective. The chemicals used included pale orange iron (III) nitrate supplied by MERCK, Germany with 99.99% purity. High purity potassium nitrate sold in white powder form by Lakshita Chemicals, India was also used. The acidity neutralizing solutions, sodium hydroxide with 99.5% purity and hydrochloric acid with 38% concentration, were obtained from China Factory Industrial, China and VWR Chemicals BDH®, England, respectively. In all experiments,

Table 1. Physical parameters

Parameter	Unit	Value	Measuring Instrument
pH	-	6.11–8.44	Portable pH meter, HI-83141-1 (Hanna-USA)
Conductivity	µS/cm	10.460–12.750	High range TDS and conductivity meter - HI99301 (Hanna-USA)
Surface tension	dyne/cm	42–56	Tensiometer, LMEC-10 (Labor Scientific Instrument Co., Ltd.-China)
Density at 20 °C	g/cm ³	1.12–1.23	AU-300SL specific gravity tester (Guangdong Hongtuo Instrument Technology Co., Ltd. -China)
Turbidity	NTU	113–153	Portable turbidity meter, HI93703 (Hanna-USA)
Viscosity	cp	1.08–1.15	Rotary viscometer, NDJ-5S (Guangdong Kejian Instrument Co., Ltd.-China)

Table 2. Chemical parameters

Parameter	Value, (ppm)	Measuring Instrument
Total suspended solid (TSS)	972–14025	Portable TSS Meter, LH-SS2M (Lianhua-China)
Total organic carbon (TOC)	1225–3520	Total Organic Carbon Analyzer, LTOC1000 (Labman-England)
Total dissolved solid (TDS)	178.180–356.000	Portable DIST 1 Waterproof TDS Tester, HI98301 (Hanna-USA)
Dissolved oxygen (DO)	7.28–8.53	Portable Optical Dissolved Oxygen Meter DO Meter, LH-DO2M(Lianhua-China)
Total petroleum hydrocarbons (TPH)	46–59	Petroleum Testing, HI932 (Hanna-USA)
Chemical oxygen demand (COD)	2684–2850	Chemical Oxygen Demand (COD) Analyzer, LH-T3COD (Lianhua-China)
Biological oxygen demand (BOD)	1000–1100	Biochemical Oxygen Demand BOD Instrument, LH-BOD606 (Lianhua-China)
Oil and grease	496–558	Gas Chromatograph-Mass Spectrometry, GCMS QP2010 (Shimadzu-Japan)
Polar compounds	150–218	Gas Chromatograph-Mass Spectrometry, GCMS QP2010 (Shimadzu-Japan)
Non-polar dissolved (NPD)	0.86–1	Gas Chromatograph-Mass Spectrometry, GCMS QP2010 (Shimadzu-Japan)
Higher acids	37–52	Gas Chromatograph-Mass Spectrometry, GCMS QP2010 (Shimadzu-Japan)
Volatile (BTX)	< 29	Gas Chromatograph-Mass Spectrometry, GCMS QP2010 (Shimadzu-Japan)
Volatile fatty acids	<20	Gas Chromatograph-Mass Spectrometry, GCMS QP2010 (Shimadzu-Japan)
Phenols	9–17	Gas Chromatograph-Mass Spectrometry, GCMS QP2010 (Shimadzu-Japan)
Polycyclic aromatic hydrocarbons (PAH)	< 0.26	Gas Chromatograph-Mass Spectrometry, GCMS QP2010 (Shimadzu-Japan)

double distilled water was used, which was prepared in the laboratory by a distillation system (2014 GFL Double distiller apparatus, Germany) at room temperature.

Stock solution of target heavy metal

In order to eschew any involvement with other contaminants, molecules and elements existing in the real produced water, the ability of almond shells to adsorb iron (III) ions was investigated using simulating solutions to the concentration of iron (III) ions in the samples of produced water mentioned in Table 4 above. A stock solution of iron (III) with a concentration of 1000 ppm

was prepared by dissolving 7.3 g of ferric nitrate nonahydrate (99% purity) of chemical formula Fe(NO₃)₃·9H₂O, supplied by Jinan Future Chemical Co., Ltd-China, in an appropriate volume of distilled water using a magnetic stirrer (Fisher Scientific, IKA™ C-MAG MS 7) at 25 ± 2 °C and 150 rpm for 20 min. After complete dissolution, the volume is accomplished up to 1 liter, and each 1 cm³ of the prepared stock solution contains 0.001 g of iron (III) ions.

Adsorbent

Almond shells collected from domestic consumption in their original form. The shells were

Table 3. Ions of produced water used in this study, measured using UV-Vis Spectrophotometer, UV-1280 (Shimadzu-Japan)

Ions	Range of concentration, (ppm)
Ammonia (NH ₄ -N)	115–182
Bicarbonate (HCO ₃ ⁻)	3078–3575
Chloride (Cl ⁻)	19.830–120.500
Sulfate (SO ₄ ⁻²)	290–1580
Sulfite (SO ₃ ⁻²)	3–10
Nitrate (NO ₃ ⁻)	1–5
Phosphate (PO ₄ ⁻³)	112–380

repeatedly washed with an ample amount of tap water to remove impurities and dirt, ensuring they were thoroughly cleaned. Afterward, they were rinsed once with distilled water. The clean shells were dried naturally in an isolated, clean place exposed to the fresh air, before being dried in a drying oven at a temperature of 40 °C until the weight was constant, to ensure that they did not char. Finally, the dried shells were collected in amber glass jars and stored in a dry location until use. Almond shells used in the current study is showing in Figure 1.

Calibration curve

For determining the mass of iron (III) ions per unit volume of treated solution, the spectroscopic method was used, where the calibration curve for the iron (III) metal, was prepared using the atomic absorption spectroscopy (AAS) device at a wavelength of 372 nm, by preparing different solutions with known concentrations of iron (III) ions. Each sample was tested, and its absorbance value was recorded. By plotting the concentration-absorbance relationship, the calibration curve required to determine the concentrations of iron (III) ions in the treated solutions was generated in this study. Figure 2 shows the calibration curve for iron (III) ions investigated in the present study.

Point of zero charge (pH_{pzc})

To determine the zero-charge point (pH_{pzc}) of almond shells, several laboratory experiments were conducted using 250 ml beakers, each containing 0.01 N solution of potassium nitrate (KNO₃), and the acidity of each beaker was adjusted using a pH meter. Solutions are prepared at different pHs, usually ranging from 1 to 14,

Table 4. Heavy metals of produced water used in this study, measured using Atomic Absorption Spectrophotometer, AA-7800 (Shimadzu-Japan)

Element	Range of concentration, (ppm)
Barium (Ba)	2.53–16.4
Cadmium (Cd)	1.7–5.2
Copper (Cu)	21–45
Mercury (Hg)	< 0.26
Lead (Pb)	5.2–12.3
Zinc (Zn)	9.45–38.7
Manganese (Mn)	0.32–11.4
Nickel (Ni)	0.86–3.5
Cobalt (Co)	0.53–2.52
Iron (Fe)	10.4–85.2
Calcium (Ca)	135–1065
Aluminum (Al)	230–388
Boron (B)	23–87
Potassium (K)	85–964
Magnesium (Mg)	1270–4310
Chromium (Cr)	< 0.88
Lithium (Li)	12–49.3
Strontium (St)	0.5–1.4
Sodium (Na)	7.326–63.540

and these values represent pH₁. A specific amount (1 g) of almond shell is then added to each sample before the flasks are placed in an agitator at 200 rpm and 25 ± 2 °C overnight, to guarantee reaching the equilibrium state. After the specified time has elapsed, the acidity of the flasks is measured, and these values represent pH₂. Then, the relationship between the difference between the



Figure 1. Almond shells utilized in current investigation

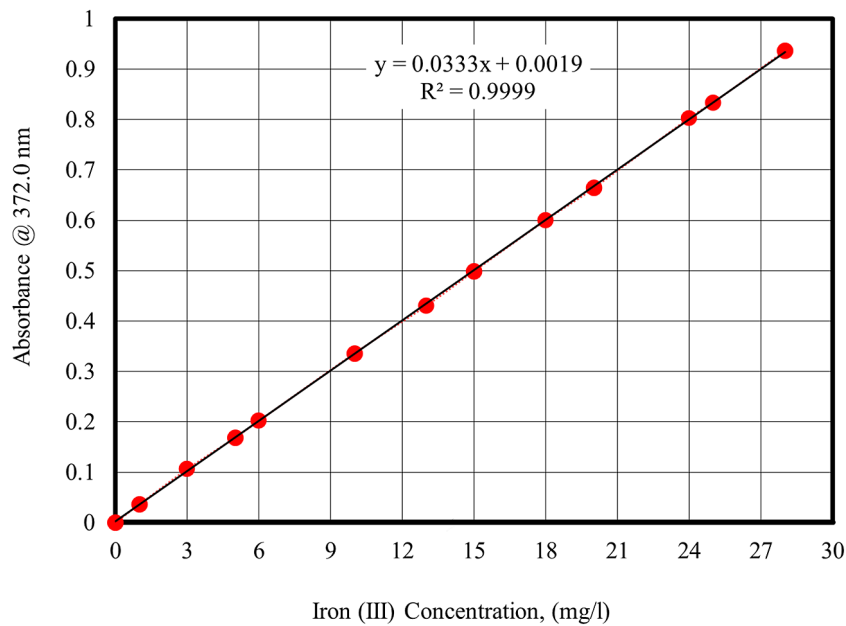


Figure 2. Calibration curve of iron (III) ions using atomic absorption spectroscopy device

initial pH and the final pH (ΔpH) versus the initial pH is plotted. At the zero-charge point (pH_{PZC}), $\Delta\text{pH} = 0$, the point where the adsorbent surface carries no net charge.

Batch adsorption unit

To reveal the optimum parameters for the recovering of iron (III) ions using almond shells as a low-cost adsorbent, a batch-type adsorption unit was used. This unit offers multiple advantages such as its convenient size, portability without the need for rebuilding, low energy consumption, no pre-treatment, and minimal additional equipment requirements. Furthermore, this unit has lower operating cost compared to continuous adsorption units. This approach allows for the efficient and precise extraction of valuable results with small, limited volumes of polluted solutions, providing a clear advantage over continuous unit that require large volumes of contaminated solutions on a continuous basis. Adsorption experiments were conducted using simulated solutions, to avoid interference with other types of pollutants found in the real polluted oil-field produced water and to apply the safety principle. The present study investigated the effect of a number of important operating conditions in any adsorption process while simulating the real conditions of oil-field produced water. The operating conditions studied were pH, agitation speed, initial concentration of iron (III) ions,

dose of almond shells, contact time, and temperature. The studied factors ranged from 2 to 9, 100–500 rpm, 10–100 ppm, 5–50 g of almond shell/liter of solution, 10–180 min, 25–50 °C, respectively. The 100 mL adsorption flasks, containing the solutions contaminated with iron ions and the specified dose of almond shells, were placed in a shaking water bath (Thermo-Fisher SHKE7000 MaxQ 7000), and a layer of aluminum foil was covering the flasks to prevent any possible interference of light on the adsorption process. After adjusting the pH value, temperature, and agitation speed, the experiment starts and continues until the specified period ends before the samples are carefully extracted and filtered from the adsorbent. The adsorption efficiency and capacity are calculated using Equations 1 and 2, respectively, after measuring the final concentration of iron (III) ions remaining at the end of the treatment process. This is done by analyzing the samples with atomic absorption spectroscopy and referring to the calibration curve presented in Figure 3.

$$q_e = (C_o - C_f) \frac{V}{m} \quad (1)$$

(2)

where: q_e – the uptake of adsorbate at equilibrium, ($\text{mg}\cdot\text{g}^{-1}$), C_o and C_f – initial, and final concentrations of adsorbate, ($\text{mg}\cdot\text{l}^{-1}$), V – volume of solution, (l), m – mass of adsorbent, (g), %R – removal percentage, (dimensionless).

RESULTS AND DISCUSSION

Zero-charge point (pH_{pzc})

It is of great importance in adsorption experiments, because it describes the interactions between the material surface and the ions in the solution as a result of a change in pH. When the solution acidity is adjusted, the adsorbent charge changes, and this change therefore affects the ability of the material for adsorption, either by attracting or repelling molecules and ions. When the pH is less than pH_{pzc} , the surface of the adsorption medium becomes positively charged, which means that it will tend to attract negative ions, and thus the adsorption of negative ions increases in this case. Conversely, when the pH is higher than pH_{pzc} , the surface of the adsorbent will be negatively charged and thus more able to attract positive ions. In the neutral case, the adsorption efficiency will be at its lowest value because the surface will then be almost neutral. Therefore, by controlling the pH value of the solution to higher or lower values than pH_{pzc} , the adsorption efficiency can be improved based on the charge of the target ions. Figure 3 represents the correlation between ΔpH and the initial pH of almond shells. It is noted from the figure above that the zero-charge point, which results from the intersection of the change in the acid function (ΔpH) with the obtained curve, is approximately 2.65. This means that the charge of the almond shells before this point is positive, i.e. it causes repulsion with the positive iron (III) ions, which leads to a decrease in the percentage removal of

the adsorption process. After 2.65, the charge of the almond shells will be negative, which is the preferred charge to attract the iron ions to be removed from the solution. By pursuit Figure 3, it is noted that the change in the pH value continues to rise until it reaches a pH value of 8, after which it begins to decrease, then it starts to decrease. This indicates that the negative charge of the almond shell surface started to decrease in contrast to the increase of the positive charge, which means that the adsorption capacity after the value of 8 will start to decrease and the pH optimum value achieves the maximum adsorption efficiency will be between 2–9. Therefore, the pH variable for removing iron ions by almond shells will be studied within this range.

Impact of acidity on the Fe^{+3} ion adsorption

Based on the result of pH_{pzc} experiments, the pH vary of the Fe(III) ion removal process from simulated aqueous solutions of produced water was studied using almond shells as a low-cost adsorbent. This parameter was studied in the range of 2–9, while the other operating conditions were kept constant at 300 rpm agitation speed, 10 ppm initial concentration, 10 g/l dosage of almond shells, 180 min contact time, and 50 °C for temperature. The results from varying this operational factor indicated that the removal efficiency improves as the acid function value increases, reaching a maximum adsorption level was 74.48% recorded at $\text{pH} = 5$, as shown in Figure 4. The reason for this result is that the charge

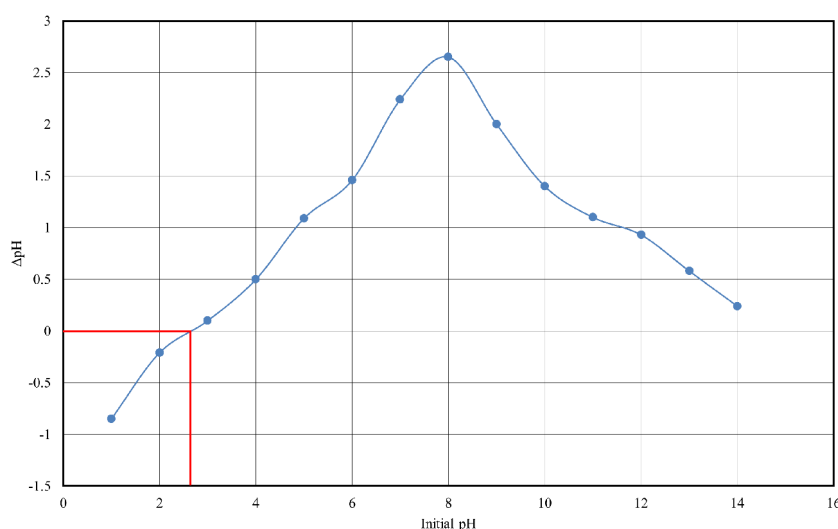


Figure 3. pH_{pzc} of almond shell used in this study

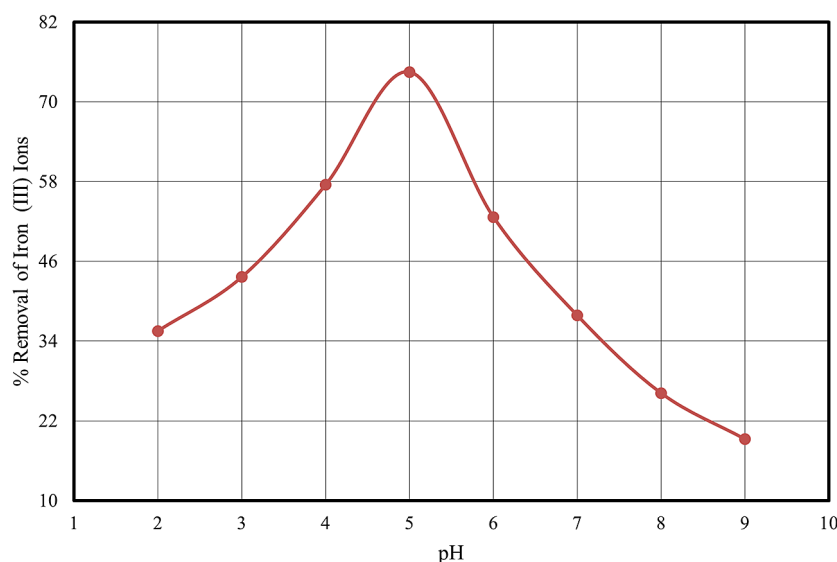


Figure 4. Effect of pH on Fe³⁺ ions removal using almond shell as an adsorbent

of the adsorption medium was negative and continuously increased with the increase of the pH value, which gives almond shells the ability to adsorb positive iron (III) ions with high efficiency. That is, the resistance that iron (III) ions will encounter during their transfer from the contaminated solution until they reach the active sites spread on the surface of the almond shells will gradually decrease with the increase in the pH value, as a result of the decrease in the value of H⁺ ions in the solution and on the surface of the adsorption medium as well, until they reach the lowest amount of resistance at pH = 5. But, after the optimum value, the adsorption efficiency begins to gradually decline with the increase of the acid function

(which is a pre-indicator from the interpretation of the zero charge point result). The decrease in efficiency is due to the fact that the surface of the material began to become positively charged as a result of the disintegration of almond shells at high pH values. This caused the surface area to decrease and the adsorbed ions to return to the solution again, which caused a decrease in the adsorption efficiency.

Impact of agitation speed on the Fe³⁺ ion adsorption

By keeping other operational variables constant at 5, 10 ppm, 10 g/l, 180 min, 50 °C for pH,

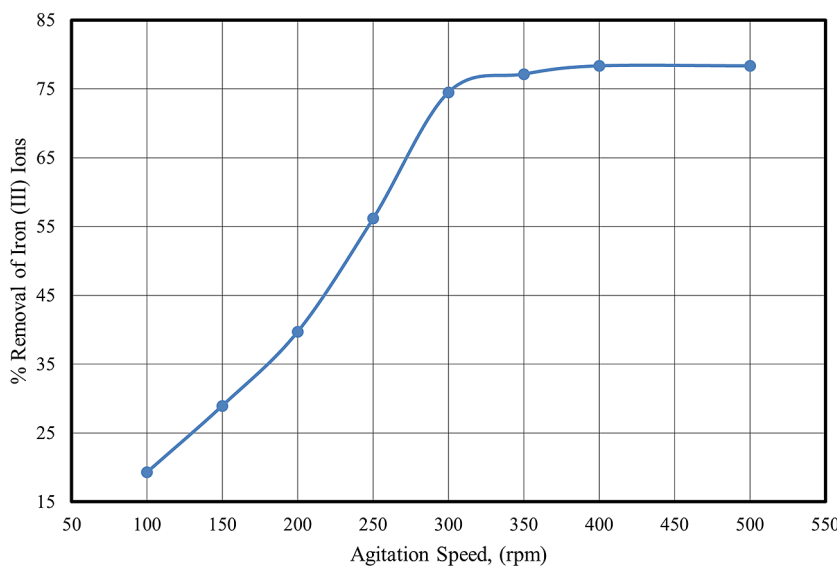


Figure 5. Effect of agitation speed on Fe³⁺ ions removal using almond shell as an adsorbent

initial concentration, almond shell dosage, contact time, and temperature, respectively, the impact of shaking on the eliminating of iron (III) ions from the contaminated solutions was studied over a range of 100–500 rpm. According to the literature and previous studies (Alsarayreh et al., 2024), these values represent the widest and most comprehensive range of studying the impact of shaking on the treatment of contaminated solutions in adsorption units operating by batch mode. The results of this variable showed that the adsorption efficiency of almond shells to adsorb iron (III) ions from aqueous solutions was directly proportional to the increase in the agitation speed and that the maximum adsorption value, which is 78.32%, was achieved at an agitation speed of 400 rpm, as shown in Figure 5. There are several explanations for this behavior, including that rising of the shaking leads to an increase in the mass transfer rate of the contaminant from the solution to the surface of the adsorption medium. Or the film layer formed on the adsorption surface will be destroyed as a result of increasing the agitation speed. Or increasing the agitation speed will cause the contaminant and the adsorbent to come closer together, as both are in motion. In all cases, this will increase the chance of capturing contaminants by the functional groups available in the active sites spread on the surface of the almond shells, leading to increased adsorption efficiency. Figure 5 confirms that the adsorption efficiency after a value of 400 rpm remains constant without any noticeable change. This result could be explained by the adsorption medium reaching the

equilibrium state, at which the rate of adsorbed particles is equal to the rate of desorbed particles, which makes the adsorption efficiency constant at the optimum value.

Impact of initial concentration on the Fe^{+3} ion adsorption

According to the experimental tests of the real samples shown in Table 4 above, the range of iron (III) ions initial concentration investigated in this study will be from 10–100 ppm. The experiments of this set were carried out by keeping other operating conditions are constant at 400 rpm, 5, 10 g/l, 180 min, 50 °C for agitation speed, pH, almond shell dosage, contact time, and temperature, respectively. Figure 6 illustrates that as the initial concentration increases, the adsorption efficiency decreases, while the relationship is directly proportional between the initial concentration and the amount of adsorbed concentration of iron (III) ions. It is obvious that any adsorption medium has a fixed surface area includes a specific number of active sites that the surrounding particles compete to occupy them according to their charge and the charge of the adsorbent surface. When the initial concentration of iron (III) ions is low, the mass of iron (III) ions will be less compared to higher concentrations, and there will be little competition between the pollutant particles to occupy the active sites, due to the limited number of particles, as a result, the concentration of iron (III) ions in the solution decreases, leading to an increase in treatment efficiency, while the

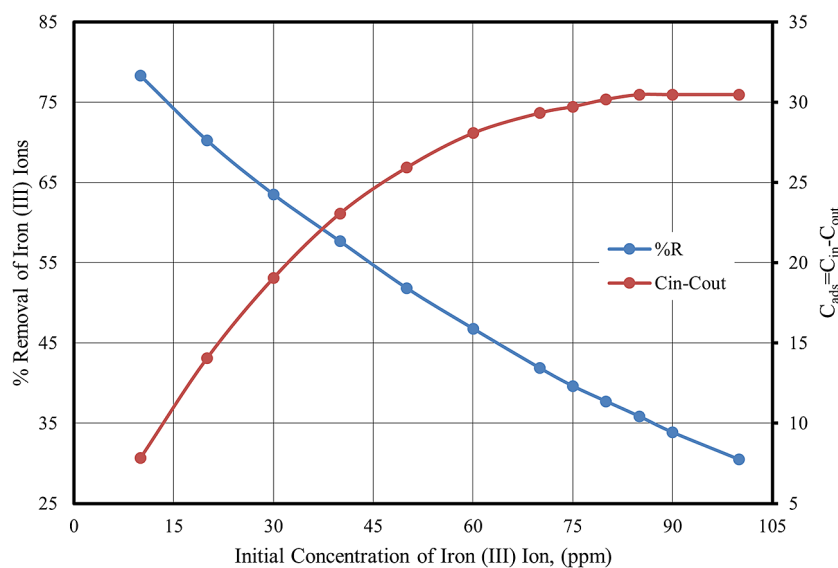


Figure 6. Effect of initial concentration of Fe^{+3} ions on % removal using almond shell as an adsorbent

adsorbed ion concentration remains low. At higher initial concentrations, the number of particles competing to occupy the same fixed number of active sites on the adsorption surface increases, intensifying the competition among particles as the initial concentration rises. As a result, the number of iron (III) ions that cannot be absorbed by the adsorption surface will increase, and they will remain spread in the solution, thus reducing the adsorption efficiency. The adsorbed concentration will gradually increase as a result of the accumulation of pollutant ions on the surface of the almond shells until it reaches its highest level, which is 30.47 ppm at initial iron (III) concentration of 100 ppm, and remains constant without change despite the rising in the initial concentration. The reason for the fixed adsorbed concentration at 85 ppm of iron ions can be explained by the almond shells reaching a state of saturation or equilibrium, which is the state in which the adsorption medium is unable to absorb any additional number of pollutants because all active sites on the surface are occupied, or as a result of the adsorption rate being equal to the desorption rate of molecules. According to the obtained results, although the adsorption efficiency is low, the optimum value of the initial concentration adsorbed by almond shells is 85 ppm.

Effect of almond shell dosage on the Fe⁺³ ion adsorption

The adsorbent dosage considers as one of the basic pillars in any adsorption process, in fact

there is no adsorption without an adsorption medium. Accordingly, determining the mass of adsorbent required to achieve maximum adsorption is of utmost importance, as it is related to reducing the cost, the resulting pressure on the unit when using more than the necessary amount, and most importantly, determining the ideal conditions that achieve the best mass transfer rate of the material. Between 5–50 g of almond shells/liter of contaminated solution, the effectiveness of this vital operating parameter was investigated, with the rest of the design variables held constant at 400 rpm, 5, 85 ppm, 180 min, 50 °C for agitation speed, pH, initial concentration of iron (III) ions, contact time, and temperature, respectively. The effect of changing the dosage of almond shells as a low-cost adsorption medium on the percentage removal of iron (III) ions from aqueous solutions is shown in Figure 7. As shown in the figure above, the adsorption efficiency increases proportionally with the rise in the mass of almond shells and that the maximum percentage removal, 96.52%, is achieved at 45 g/L. Raising the adsorbent dose results in a larger surface area of the almond shells being available for adsorption, which providing additional active sites for the same number of iron (III) ions due to the constant concentration, which in turn leads to reducing the competition between the ions for those sites, and thus the adsorption surface will be able to absorb a larger number of iron (III) ions. Therefore, its concentration in the solution decreases, leading to an increase in efficiency. Additionally, it is observed that the adsorption efficiency stabilizes

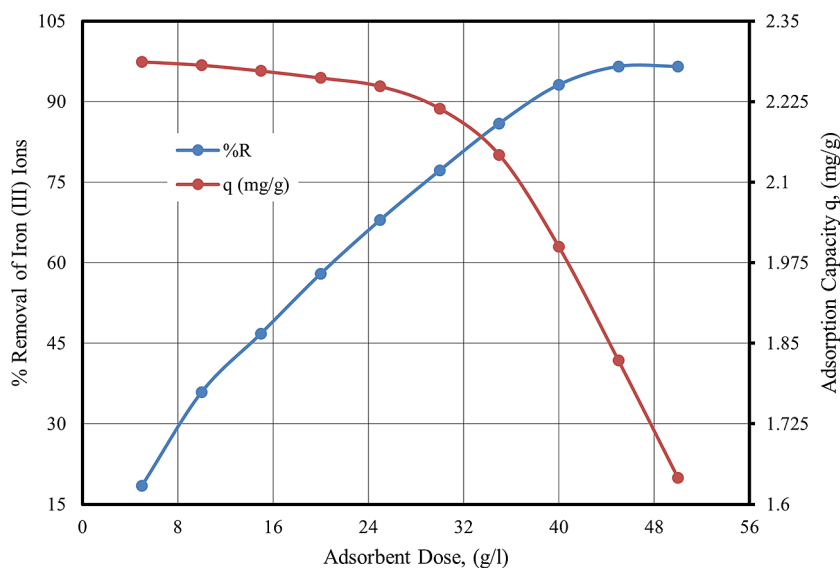


Figure 7. Effect of adsorbent dose on Fe⁺³ ions removal using almond shell as an adsorbent

and remains unchanged after 45 g/l, which may be attributed to the fact that the almond shells reach a saturation state, at which point they are unable to adsorb any more iron (III) ions. Therefore, the optimum dose of almond shells required to adsorb the maximum mass of iron (III) ions is 45 g/l under the specified operating conditions.

Impact of contact time on the Fe⁺³ ion adsorption

The time between 10–180 minutes is considered the optimum time range for studying adsorption in batch-type systems, as time less than 10 minutes is too short and the adsorption kinetics cannot be understood. While the time after 180 minutes is very long and requires additional cost resulting from energy consumption, in addition to the many imperceptible changes that may occur to the adsorbent during this period of time. In this time range, and keeping remaining operating conditions constant at 400 rpm, 5, 85 ppm, 45 g/l, 50 °C for agitation speed, pH, initial concentration of iron (III) ions, adsorbent dose, and temperature, respectively, this important design parameter characterized the kinetics of iron (III) ions adsorption process using almond shells as a low-cost adsorbent. The obtained results, which are represented in Figure 8 demonstrates that extending the contact time enhances the adsorption efficiency, with approximately 10% of the target material being removed within the first 10 minutes of interaction between the iron (III) ion-contaminated solution and almond shells. The

highest adsorption efficiency was achieved at 150 minutes. Prolonging the contact time increases the likelihood of pollutant ions reaching the adsorbent surface, which in turn improves their interaction with the active sites and functional groups, leading to greater treatment efficiency as the pollutant concentration in the solution decreases. After 150 minutes, the adsorption efficiency stabilizes at 96.52%, remaining unchanged despite the continued treatment. This plateau suggests that the almond shells have reached their saturation point and can no longer adsorb additional iron (III) ions. Therefore, 150 minutes is considered the optimal time for maximizing the removal of iron (III) ions from contaminated aqueous solutions using almond shells as a cost-effective adsorbent.

Impact of temperature on the Fe⁺³ ion adsorption

The temperature effect on iron (III) ions from simulated produced water contaminated aqueous solutions using almond shells was studied over a range of 25–50 °C, with the rest of the variables held constant at the optimum values. Experimental results from the study of this important factor, clarified by Figure 9, showed that the treatment is low at low temperatures, and that the efficiency of the adsorption process improves with increasing temperature, and the percentage of removal gradually increases with increasing temperature from approximately 12% at 25 °C to 96.5% at 50 °C, which is the maximum value. Increasing the temperature increases the kinetic energy of the iron

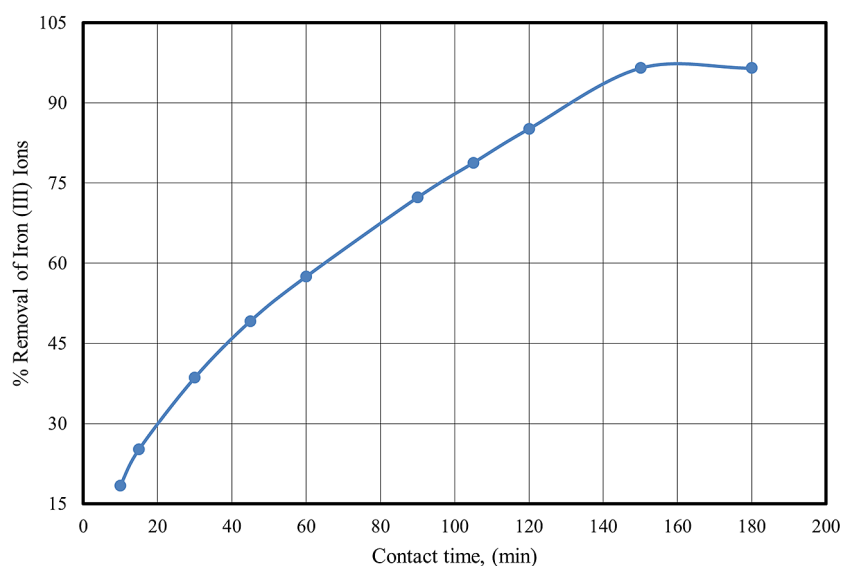


Figure 8. Effect of contact time on Fe⁺³ ions removal using almond shell as an adsorbent

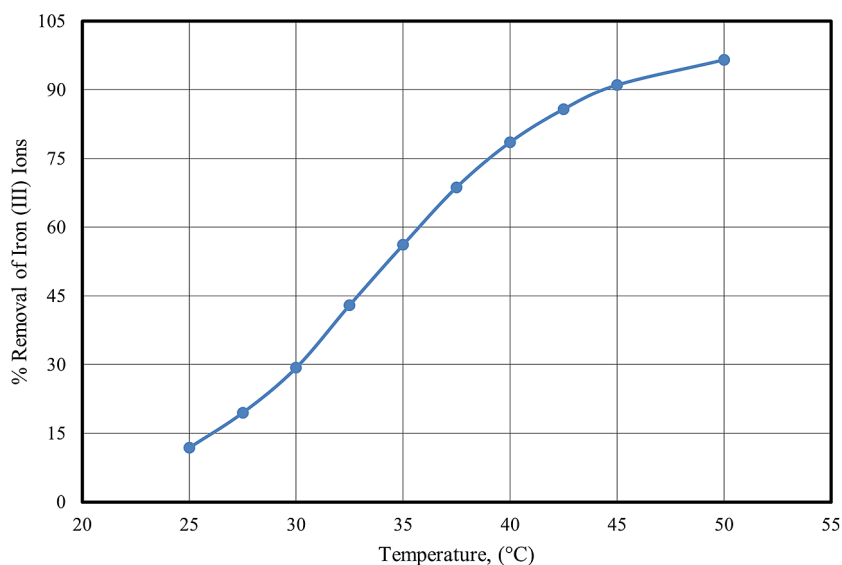


Figure 9. Effect of temperature on Fe^{+3} ions removal using almond shell as an adsorbent

(III) ions, which increases the mass transfer rate of the target ions in the solution and brings it closer to the almond shells. This, in turn, enhances the likelihood of contaminated ions binding to the functional groups on the active sites of the adsorption surface, thereby improving treatment efficiency. Furthermore, raising the temperature can modify the adsorption surface by expanding the pores on the almond shells, facilitating greater access for the targeted ions to the active sites and promoting their interaction with the functional groups, which boosts adsorption efficiency. Additionally, increased temperature may alter the chemical structure of the molecules or the adsorbent surface, thereby increasing the reactivity of the molecules and enhancing the adsorption rate.

Fourier-transform infrared spectroscopy (FTIR) test

FTIR spectroscopy is a powerful tool used to identify the functional groups present on the surface of the adsorbent before and after adsorption, and through these spectra, the structural changes on the surface after the adsorption process can be determined. Based on Figure 10, which represents the FTIR spectrum of almond shells before adsorption, the shells contain functional groups such as hydroxyl (-OH), carbonyl (C = O), and ethers (C-O), which show strong absorption peaks. After adsorption, a significant decrease in the intensity of the absorption peaks and slight shifts in their positions are observed, indicating a direct interaction between these functional groups and iron

ions. As a result, it can be said that almond shells showed a clear ability to adsorb iron (III) ions. In the region between $3500\text{--}3200\text{ cm}^{-1}$ which represents (O-H Stretching), a broad peak appears in this region before adsorption (blue spectrum), indicating the presence of hydroxyl groups (-OH) on the surface of almond shells, whether from the absorbed water or from the original hydroxyl groups in the shells. After adsorption (red spectrum), a significant decrease in the intensity of this peak is observed, indicating the interaction of -OH groups with iron ions. This decrease suggests that -OH groups participated in the adsorption process or that water molecules were replaced by ions. In the region $3000\text{--}2850\text{ cm}^{-1}$ (C-H Stretching), there is a weak peak indicating the presence of alkane C-H bonds in the shells before adsorption. After treatment with iron (III) ions, this peak weakens significantly, which may indicate slight changes in the organic structure, or that the adsorption affected the organic groups attached to the carbon skeleton. (C=O Stretching - Carbonyl Groups) represents the region between $1740\text{--}1600\text{ cm}^{-1}$, here a strong absorption appears before desorption indicating the presence of carbonyl groups (C=O) such as carboxyl or ester. This absorption is slightly weakened after adsorption in intensity, with a slight shift in the location of this peak. This shift and change in intensity indicate that the carbonyl groups have interacted with the iron (III) ions during the adsorption process. The band at $1600\text{--}1500\text{ cm}^{-1}$ shows the functional group (C=C aromatic stretching), in this region, before adsorption, a peak indicating

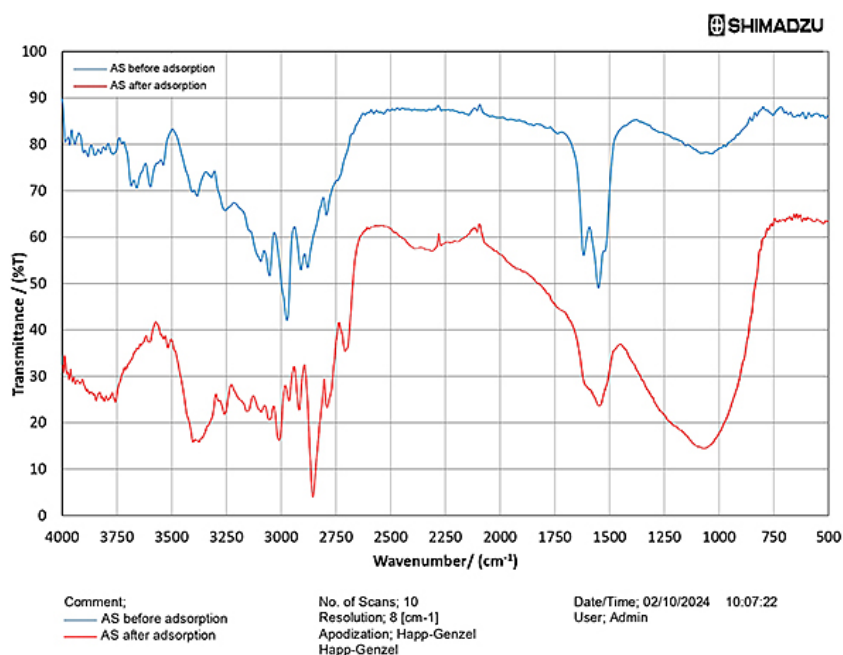


Figure 10. FTIR spectra of almond shell before and after adsorption of Fe⁺³ ions

C=C bonds in aromatic rings is observed, while the same peak after adsorption suffers from slight changes in the shape of this peak, which may indicate the occurrence of an interaction between iron ions and aromatic groups in almond shells. The region between 1250–1000 cm⁻¹ is (C-O stretching), before adsorption, a strong peak is observed in this range indicating C-O stretching, possibly in ether or hydroxyl groups. After adsorption, a change in the peak position and intensity occurs, indicating the interaction of C-O groups with iron (III) ions, which is an indication of the ions' attachment to these functional groups on the surface of the scales. The final region limited between 900–500 cm⁻¹ (called Finger Print Region). This region is known as the fingerprint region, and is very sensitive to changes in molecular structure. It can be observed that there are large changes in this region after adsorption, indicating structural changes in the shells due to their interaction with iron ions.

Surface area test

Surface area testing of adsorbents is essential to determine the adsorption capacity of adsorbents and their use in water treatment applications, catalysts, etc. The Brunauer-Emmett-Teller (BET) technique is commonly used to measure surface area. This test is performed by exposing the sample to a gas (usually a mixture of nitrogen

and helium) under low pressure at a certain temperature. After the gas is adsorbed on the surface of the material, the volume of gas adsorbed on the surfaces of the particles is calculated, and based on this data the exact surface area of the sample is calculated. This process gives insight into the adsorption efficiency of materials and improves their performance, as larger surface area means higher adsorption efficiency, which is important in applications such as water and air treatment, and chemical processes. The surface area of the adsorption medium was investigated in this study using BET technique and using a mixture of helium and nitrogen gas. The results obtained showed that virgin almond shells have a surface area estimated at 7.7 m².g⁻¹, as in Figure 11, which reflects the ability of these shells to provide a simple but suitable surface area for treating pollutants, and thus they can be used as an adsorption medium effectively. However, after the adsorption process was completed, the surface area decreased to 0.73 m².g⁻¹, indicating that many of the available gaps for reaction had been closed due to the binding of iron (III) ions to the active sites spread on the surface exposed to adsorption. This significant decrease in surface area indicates that almond shells were able to adsorb a significant amount of iron (III) ions, reflecting the efficiency of the adsorption process. In addition, a decrease in surface area may be an indication of changes in the internal structure of the crust, which may affect

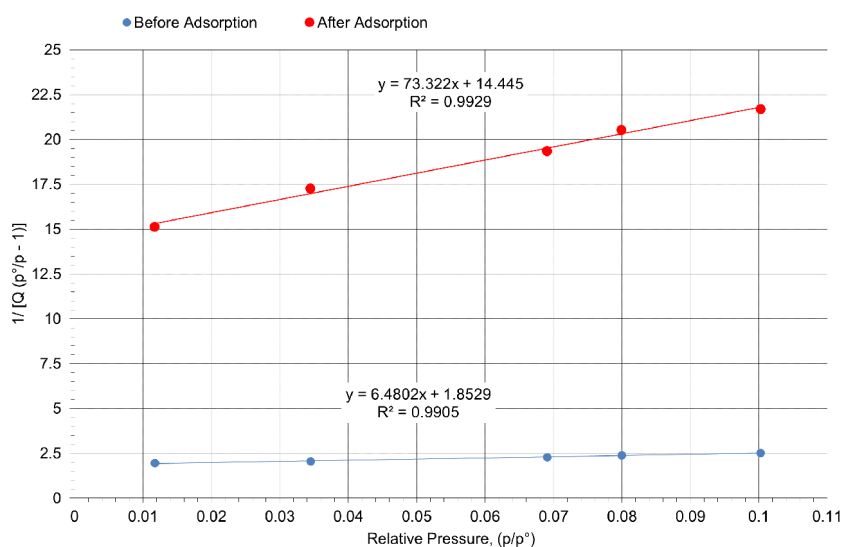


Figure 11. BET surface area test of almond shells before and after adsorption of Fe³⁺ ions

the physical and chemical properties of the surface. These results support the importance of using almond peels as effective adsorbents in water treatment, as they contribute to the removal of metal pollutants by forming new bonds between iron (III) ions and the surface of the peels.

Scanning electron microscopy test

Scanning electron microscopy (SEM) is an advanced analytical tool used to image and examine surfaces at the molecular and sub-molecular level. The technique relies on scanning the surface of a sample with a beam of electrons, where the resulting image is magnified by detectors that capture secondary or background electrons emitted by the sample. The importance of this technique lies in its ability to provide accurate information about surface morphology, including the shape, size, and distribution of gaps, defects, and texture. Figure 12 shows the SEM examination of virgin almond shells before adsorption, where the surface structure reveals parallel lines that extend regularly, giving the surface a unique appearance. The pores on the surface are regular, but vary in shape, reflecting the complexity of the plant tissue of almond shells. The overall composition is homogeneous, indicating the preservation of the natural structure of virgin shells, which enhances the function of the shells as an adsorbent. This structural homogeneity of the plant tissue emphasizes the unity of chemical and physical composition, providing an important basis for the use of this type of peel as a natural, low-cost adsorption medium. Figure 13 represents the SEM examination

of almond shells after adsorption, and it is noted that there are clear changes in the surface structure as a result of their interaction with iron (III) ions. The texture of the shells became more random and irregular, reflecting the effect of adsorption on the surface structure. The pores, which were previously small and regular, have decreased in number due to fusion and have expanded in size and become irregular, indicating changes in the chemical composition due to the adsorption of ions. The previously characteristic filamentous arrangement of the surface has disappeared, replaced by spherical structures of various shapes, indicating the formation of new bonds between iron (III) ions and the plant surface. These features of almond shells after adsorption supported

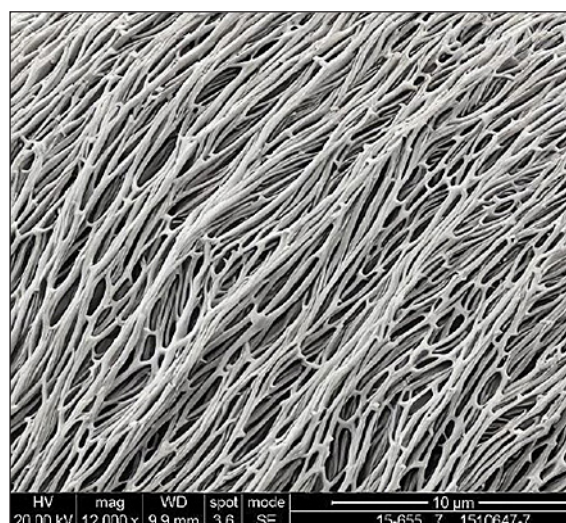


Figure 12. SEM image of almond shells before adsorption of iron (III) ions

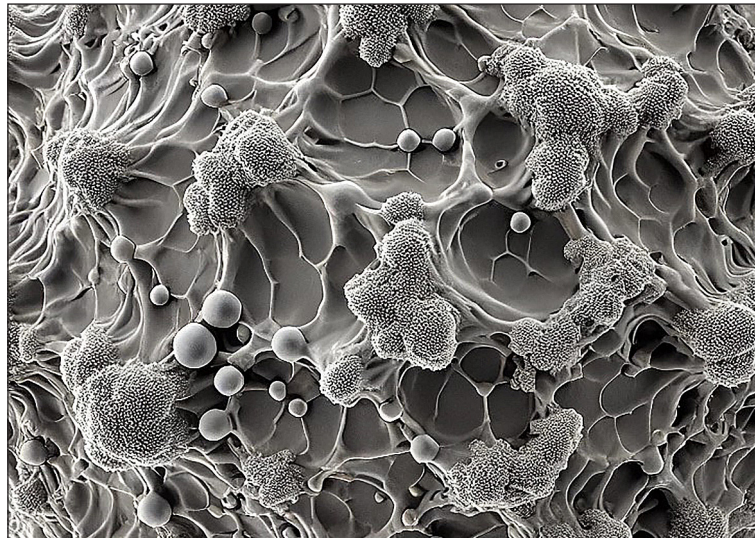


Figure 13. SEM image of almond shells after adsorption of iron (III) ions

the results obtained from varying the temperature above, which confirmed that the increase in adsorption efficiency with increasing temperature may be due to the expansion of the surface gaps and pores of the shells to enable them to adsorb a greater number of ions. These changes largely reflect the ability of almond shells to adsorb iron (III) ions, making them an effective material for removing pollutants from solutions as a low-cost natural adsorption medium.

Behavior of adsorption

The adsorption behavior of iron (III) ions using almond shells as a low-cost adsorbent can be determined through a three-sections study: isothermal study, which studies the correlation between the amount of adsorbent and the concentration at constant temperature; kinetic study, which explores the adsorption rate and mechanisms; and thermodynamic study, which reveals the nature of the energetic interactions, like changes in enthalpy and Gibbs free energy.

Isothermal study

It is regarded as a crucial factor for understanding the adsorption behavior at equilibrium, as it illustrates the relationship between the mass of the adsorbent and the concentration of the adsorbate in either the liquid or gas phase at a constant temperature. This study allows determining the surface adsorption capacity and clarifying the nature of the interactions that occur at the surface. The isothermal study is based on a set of

mathematical models that explain the relationship between the concentration of the adsorbent and the amount of adsorption. By applying these models, the efficiency and adsorption capacity of the adsorbent can be evaluated, and the suitability of the model to the adsorption data obtained from practical experiments can be determined. The current study used three models, which are considered the most important types. The first model is Langmuir Isotherm Model, which is one of the most common models, and it is based on the assumption that adsorption takes place on a uniform surface, with all adsorption sites having the same energy, and that the adsorption occurs in a monolayer. This model also assumes that there is no interaction between the adsorbed molecules. The other model is Freundlich Isotherm Model, which is an experimental model utilized for heterogeneous surfaces, which assumes unequal adsorption energy at all sites. This model is suitable for multilayer adsorption processes, and shows variation in the ability of the adsorbent to adsorb over a wide range of concentrations. The third model is Temkin Isotherm Model, which is used to characterize heterogeneous systems, with the assumption that the adsorption rate decreases as surface coverage increases, due to the reduction in available energy for adsorption. Table 5 shows the general and linear mathematical formulas for the isothermal models used to clarify the adsorption of iron (III) ions using almond shells.

Figures 14–16 and Table 6 show the results obtained from applying these isothermal models to the empirical results for adsorption of iron (III) ions using almond shells as a low-cost adsorption

Table 5. Details of isothermal models

Model	General form	Linear form	Slop	Intercept	Augmented parameter
Langmuir	$q_e = \frac{q_{max} \cdot K_L C_e}{1 + K_L C_e}$	$\frac{1}{q_e} = \frac{1}{q_{max} K_L C_e} + \frac{1}{q_{max}}$	$\frac{1}{q_{max} K_L}$	$\frac{1}{q_{max}}$	$R_L = \frac{1}{1 + K_L C_e}$
Freundlich	$q_e = K_F C_e^{\frac{1}{n}}$	$\ln q_e = \ln K_F + \frac{1}{n} \ln C_e$	$\frac{1}{n}$	$\ln K_F$	-
Temkin	$q_e = \frac{RT}{b} \ln K_T C_e$	$q_e = \frac{RT}{b} \ln K_T + \frac{RT}{b} \ln C_e$	$\frac{RT}{b}$	$\frac{RT}{b} \ln K_T$	-

Note: q_e – adsorption capacity at equilibrium state (mg.g⁻¹), C_e – equilibrium adsorbed concentration (mg.g⁻¹), q_{max} – maximum adsorption capacity of Langmuir model (mg.g⁻¹), K_L – constant of Langmuir adsorption isotherm model, expressed the binding sites (l.mg⁻¹), R_L – separation factor in Langmuir model (dimensionless), K_F : constant of Freundlich adsorption isotherm model (mg.g⁻¹).(l.mg⁻¹)^{1/n}, n – intensity of the adsorption in Freundlich model (dimensionless), K_T – Temkin isotherm equilibrium binding constant (l.mg⁻¹), R – universal gas constant (8.3144 J.mol⁻¹.K⁻¹), b – constant in Temkin isotherm model (dimensionless), and T – absolute temperature (K).

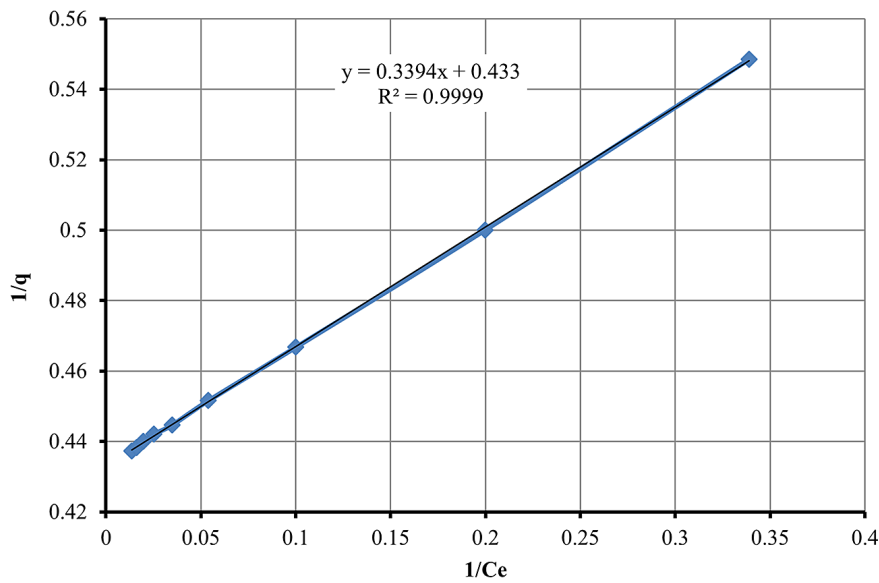


Figure 14. Langmuir isotherm model

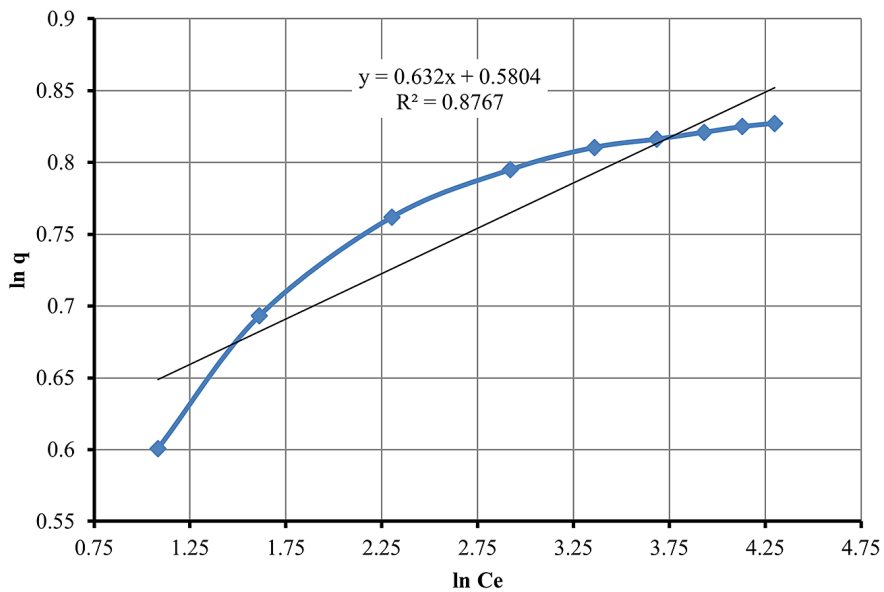


Figure 15. Freundlich isotherm model

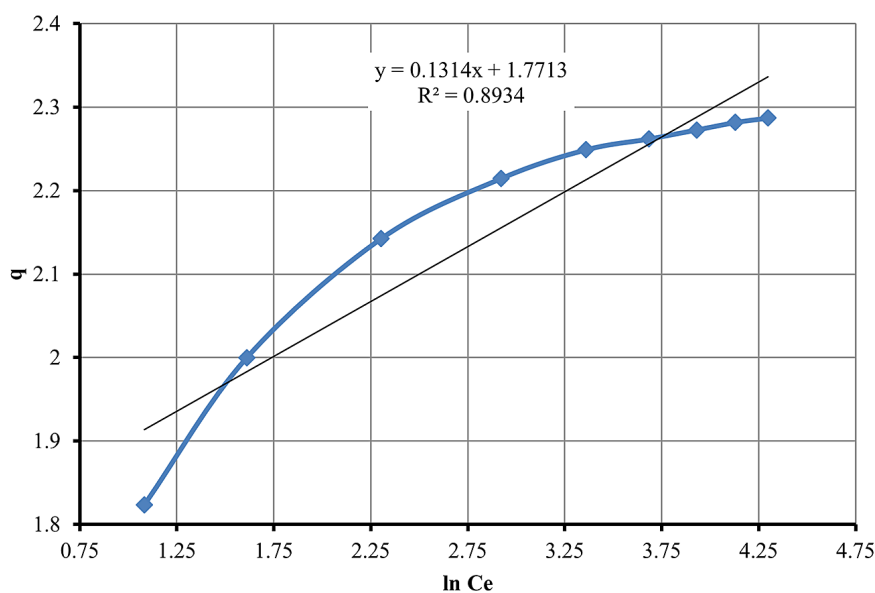


Figure 16. Temkin isotherm model

medium. It is clear from the figures and table above that the Langmuir model best reflected the experimental results, due to the high correlation coefficient (R^2) value that is very close to the ideal value, while the Freundlich and Temkin models were inefficient in describing the adsorption isotherm, as their correlation coefficients were 0.8767 and 0.8934, respectively. The interpretation of this result means that the adsorption takes place in a monolayer on a uniform surface, with all adsorption sites having the same energy level, which was confirmed by the SEM test, which showed that almond shells have an organized and homogeneous surface with pores of similar size.

Adsorption kinetics study

It seeks to assess the adsorption rate and the mass transfer mechanism from the solution or gas to the adsorbent surface. Kinetic analysis aids in evaluating the adsorption rate and identifying the factors influencing it, including the characteristics of the adsorbent surface, adsorbate concentration, and temperature. The study is based on a set of kinetic models that describe the adsorption behavior over time and help in predicting interactions of the surface. Several models were used to describe

the adsorption kinetics of iron (III) ions on the surface of almond shells, namely, Pseudo First Order Model, which posits that the adsorption rate is directly related to the difference between the equilibrium adsorption amount and the quantity adsorbed at any specific time. It is used primarily for physical adsorption. The second model is Pseudo Second Order Model, which supposes the adsorption rate depends on the square of the difference between the amount of adsorption at equilibrium and the amount adsorbed. It is most suitable for chemical adsorption processes where there is an interaction between the adsorbent and the adsorbate. The other model is Elovich model, which is used to describe heterogeneous systems, and it is assumed that the adsorption rate decreases with increasing surface coverage due to the decrease in the energy available for adsorption. The last one is Intra-particle diffusion model, which focuses on the effect of the adsorbent diffusion within the adsorbent molecules. This model is used when the adsorption process is limited by the transport of molecules within the adsorbent and not only on its surface. Table 7 shows the differential and linear mathematical formulas for the

Table 6. Constants of isothermal models used in the current study

Langmuir isotherm model				Freundlich isotherm model			Temkin isotherm model		
q_{max}	K_L	R_L	R^2	K_F	n	R^2	K_T	b	R^2
2.3095	1.2758	0.0091	0.9999	1.7868	1.5823	0.8767	1.0138	20.4465	0.8934

Table 7. Details of kinetic models

Kinetic Model	Differential form	Linear form	Slop	Intercept
Pseudo first order	$\frac{dq_t}{dt} = k_1(q_e - q_t)$	$\ln(q_e - q_t) = \ln q_e - k_1 t$	$-k_1$	$\ln q_e$
Pseudo second order	$\frac{dq_t}{dt} = k_2(q_e - q_t)^2$	$\frac{t}{q_t} = \frac{1}{k_2 q_e^2} + \frac{1}{q_e} t$	$\frac{1}{q_e}$	$\frac{1}{k_2 q_e^2}$
Elovich model	$\frac{dq_t}{dt} = \alpha e^{-\beta q_t}$	$q_t = \frac{1}{\beta} \ln t + \frac{1}{\beta} \ln \alpha \beta$	$\frac{1}{\beta}$	$\frac{1}{\beta} \ln \alpha \beta$
Intra-particle diffusion	–	$q_t = k_p t^{0.5} + C$	k_p	C

Note: q_e – adsorption capacity at equilibrium state (mg.g⁻¹), q_t – adsorption capacity at any time (mg. g-1), k_1 – first order rate constant (min⁻¹), k_2 – second order rate constant (g mg⁻¹ min⁻¹), α – initial adsorption rate in Elovich model (mg g⁻¹ min⁻¹), β – desorption constant in Elovich model (g mg⁻¹), k_p – rate constant in intra-particle diffusion model (mg g min^{-0.5}), and C – thickness of boundary layer (mg.g⁻¹).

kinetics models used to describe the adsorption of iron (III) ions using almond shells.

Figures 17–20 and Table 8 show the results obtained from applying these kinetic models to the experimental data for the adsorption of iron (III) ions using almond peels as a low-cost adsorption medium. It is clear from the figures and table above that the intra-particle diffusion model is the closest to representing the experimental results with a slight advantage over the pseudo-second-order kinetic model according to the correlation coefficient which was 0.9999 and 0.9967 for these two models, respectively. From the assumptions of this model, the adsorbate moves inside the almond shells, therefore requires a greater momentum than the normal case. This was confirmed by the results of the agitation speed, which shows that the highest adsorption efficiency achieved at optimum

speed which was 400 rpm, which is a high speed, meaning that the arrival of iron (III) ions to the active sites on the surface of almond peels requires the destruction of the film layer formed on the adsorption surface. As for the second pseudo-order kinetic model and Elovich model, their representation was not identical to the results obtained according to the correlation coefficient (R²), which had values of 0.9753 and 0.9471, respectively.

Adsorption thermodynamic study

The thermodynamic study of adsorption aims to analyze the energy involved in the adsorption process and determine the nature of the interactions that occur between the adsorbent and the adsorbent. Through this study, the basic thermodynamic

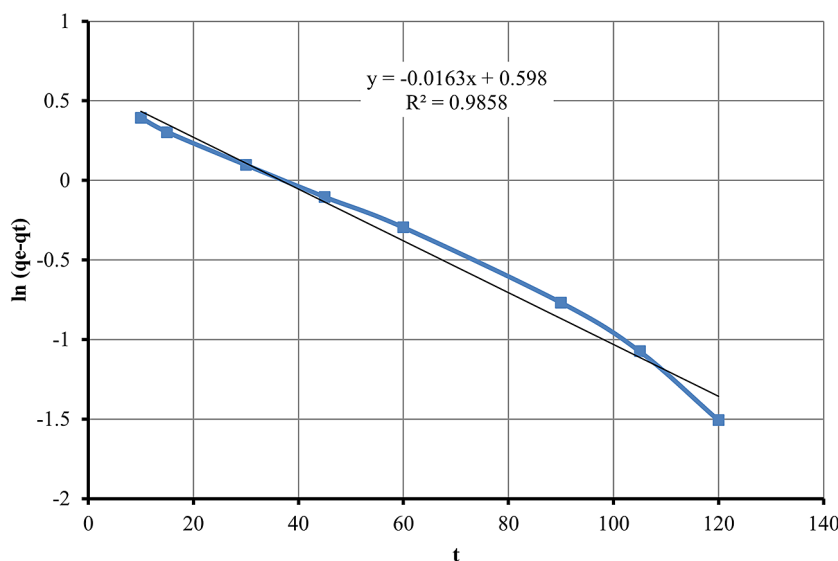


Figure 17. Pseudo first order kinetic model

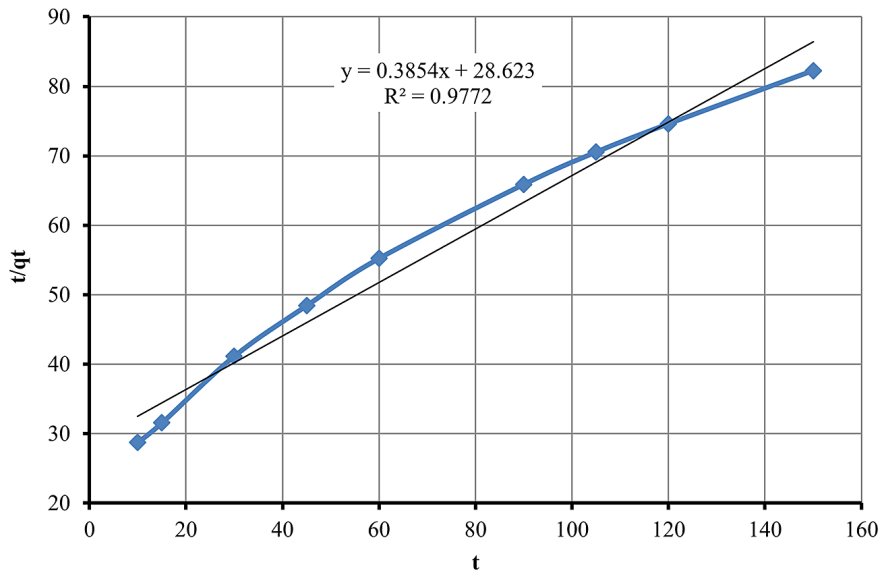


Figure 18. Pseudo second order kinetic model

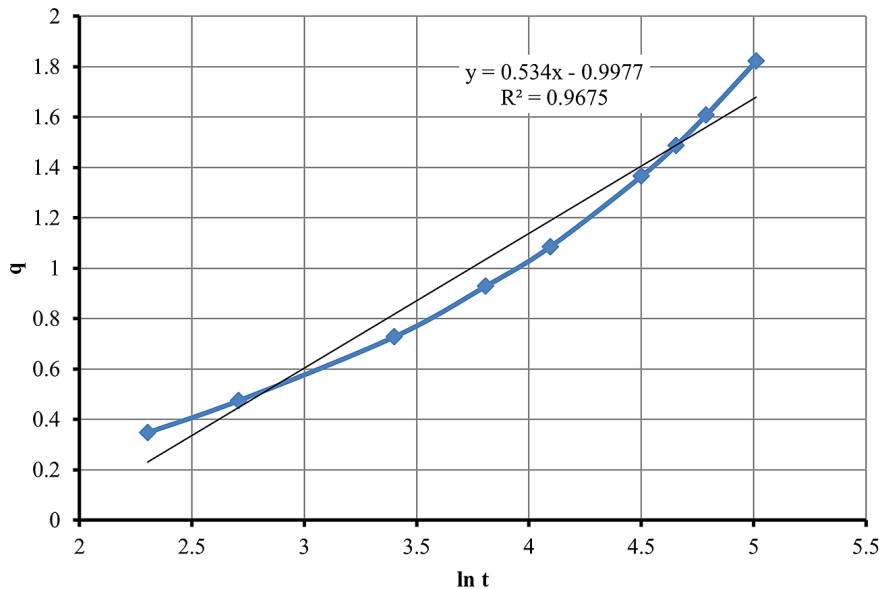


Figure 19. Elovich kinetic model

parameters are calculated, i.e. the change in free energy (ΔG), which determines the spontaneity of the process, as adsorption occurs spontaneously if the value of ΔG is negative. In addition, the value of the change in enthalpy (ΔH) can be calculated also, which indicates the extent of energy absorption or release during adsorption. If ΔH is negative, the adsorption is exothermic, and if it is positive, it is endothermic. The last thermodynamic factor is the change in entropy (ΔS), which reflects the degree of randomness or disturbance in the system after adsorption. An increase in entropy (ΔS is positive) indicates increased disorder at the surface. The calculation of these coefficients depends on adsorption

data at different temperatures, and then apply the Van't Hoff equation, shown in Equation (3), to compute the changes in enthalpy (ΔH), entropy (ΔS), and Gibbs free energy (ΔG), using the adsorption equilibrium constants at several temperatures.

$$\Delta G = \Delta H - T\Delta S \tag{3}$$

$$\ln k_{ad} = -\frac{\Delta H}{R} \frac{1}{T} + \frac{\Delta S}{R} \tag{4}$$

where: k_{ad} – adsorption equilibrium coefficient (-); R – universal gas constant (8.3144 J/mol.K); T – absolute temperature (K); ΔH – enthalpy change (kJ/mol); ΔS – entropy change (J/mol.K); ΔG – Gibbs free energy (kJ/mol).

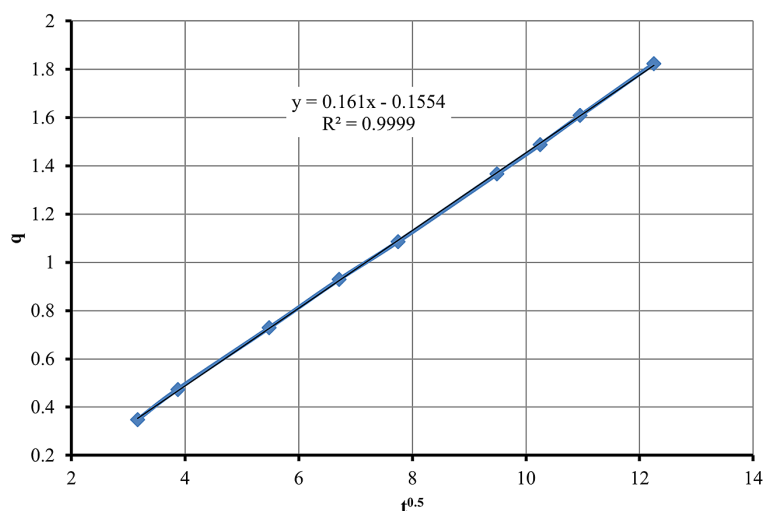


Figure 20. Intra-particle diffusion kinetic model

Table 8. Constants of kinetics models

Pseudo first order			Pseudo second order			Elovich model			Intra-particle diffusion		
k_1	q_e	R^2	k_2	q_e	R^2	α	β	R^2	k_p	C	R^2
0.0163	1.8185	0.9858	0.0052	2.5947	0.9772	3.459	1.8727	0.9675	0.161	-0.1554	0.9999

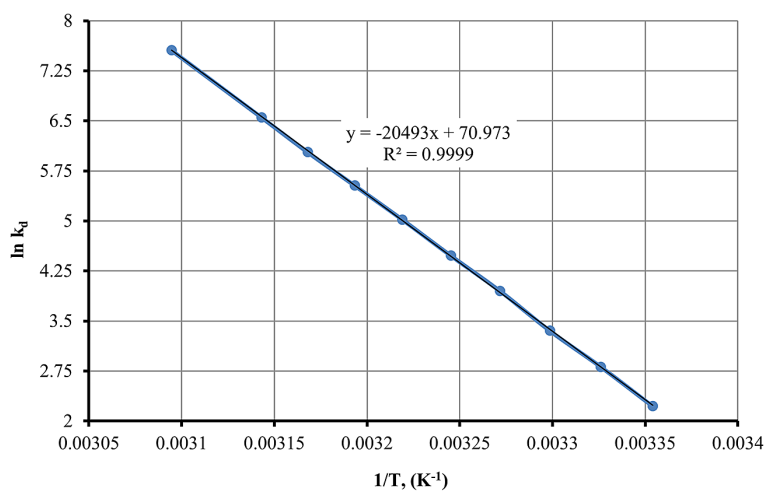


Figure 21. Thermodynamic behavior for Fe³⁺ adsorption using almond shells

The plot of logarithmic distribution coefficient ($\ln k_d$) against ($1/T$) in Figure 21, as described in Equation 4, was used to determine the thermodynamics parameters ΔH and ΔS from the slope and intercept, respectively, while Table 9 show the results of iron adsorption on almond shell. It's clear that the adsorption process of iron (III) ions on almond shell as low-cost adsorbents is spontaneous, as evidenced by the negative values of ΔG° . The positive sign of ΔH° indicates that the adsorption

process is endothermic within temperature range between 25–50 °C, implying that as temperature rises, adsorption efficiency rises this might be owing to the adsorbent surface's creation of additional active sites, as well as the enhanced rate of pore diffusion. Also, the adsorption is of chemical type due to the value of enthalpy. Additionally, the positive ΔS refers to greater randomness at the solid/solution interface during the adsorption process. Similar results reported by (Alhamed et al., 2024a).

Utilizing from the almond shell residue loaded with iron (III) ions

After determining the efficacy of almond shell for iron (III) ions in aqueous solutions, the later step involved the safe disposal of this toxic-loaded remnants in eco-friendly method. One proposed approach involved using these toxic residues as an additive in the concrete mix to improve its performance by evaluating the compressive strength both before and after the addition. To carry out this procedure, three types of concrete mixtures were prepared. The first mixture served as a reference, with a mixing ratio of 4:2:1 (gravel:sand:cement) and a water-to-cement ratio of 0.45. The second mixture followed the same proportions but included 2% virgin almond shell by weight. The last type was the same second type, but adding Fe⁺³-almond shell by ratios ranged between 0.1–3.0% of the mixture. Table 10 details of the concrete mixtures used in the study.

The cement used in this study was ordinary Portland type produced from Tasluja - Iraqi origin bazian, while the sand (fine aggregates) and gravel (coarse aggregates) were supplied from Al-Ukhaidir region, south-west of Baghdad and Al-Nebai region, north-west of Baghdad, respectively. All components are complying with the Iraqi standard of 1984. Drinking water from tap has been employed to prepare the concrete mixture.

Testing method (compressive strength test)

The compressive strength of concrete used in structural applications is typically represented by the force (stress) in Newtons required to cause failure, divided by the area in square millimeters (mm²). The compressive strength of the concrete

mixture is determined using a 0.15 × 0.15 × 0.15 m cube sample or a cylindrical sample with a height twice its diameter. The treatment is conducted using the wet method for 7- and 28-days, following the Iraqi specifications at laboratory temperature. The sample is placed in a standard concrete compressive strength testing machine and subjected to a specific loading rate until it ruptures. The loading process typically takes 2–3 minutes to complete. In this study, the compressive strength test was conducted in accordance with the British Standard Specification (B.S. 1881: Part 116) on concrete cubes at 7 and 28 days. The tests were performed using a 2500 kN capacity compressive strength testing machine (WeKob) with a load rate of 15 MN·m⁻²·min⁻¹, continuing until the sample began to rupture. Cubes of the reference concrete mixture and concrete mixtures with additives were tested at different ages (7- and 28-days) to determine the optimal compressive strength. The compressive strength measured was the average value of three cubes for each test at each age. It is obvious from Figure 22 the enhanced effect of iron (III) loaded almond shell to concrete mixture behavior. The compressive strength of the cubes steadily increased from 33.71 kN/mm² at a 0.1 ratio to a peak value of 51.23 kN/mm² at a 2 ratio. This enhancement in compressive strength of the concrete mixture, resulting from the incorporation of almond shells loaded with iron (III) ions, could be attributed to the improved adhesion between the iron-loaded almond shells and the cement in the concrete. The adhesion is influenced by the physical and chemical properties derived from the almond shell's structure. Furthermore, the compressive strength in this case improved due to the presence of iron (III) ions on the almond shell surface. Iron (III), being a high-density

Table 9. Thermodynamic parameters of Fe⁺³ adsorption using almond shells

Temperature, (K)	ΔH (kJ/mol)	ΔS (J/mol.K)	ΔG (KJ/mol)
298.15	170.3882	590.1024	-5.5507
300.65			-7.02600
303.15			-8.5013
305.65			-9.9765
308.15			-11.4518
310.65			-12.9270
313.15			-14.4023
315.65			-15.8775
318.15			-17.3528
323.15			-20.3033

Table 10. Details of the concrete mixtures used in the study

Type of mixture	Cement, kg/m ³	Sand, kg/m ³	Gravel, kg/m ³	W/C, ratio	% wt. of almond shell (AS) added
Reference	300	600	1200	0.45	-
Mixture 1	300	600	1200	0.45	2.0% of AS
Mixture 2	300	600	1200	0.45	0.1–3.0% Fe ⁺³ -AS

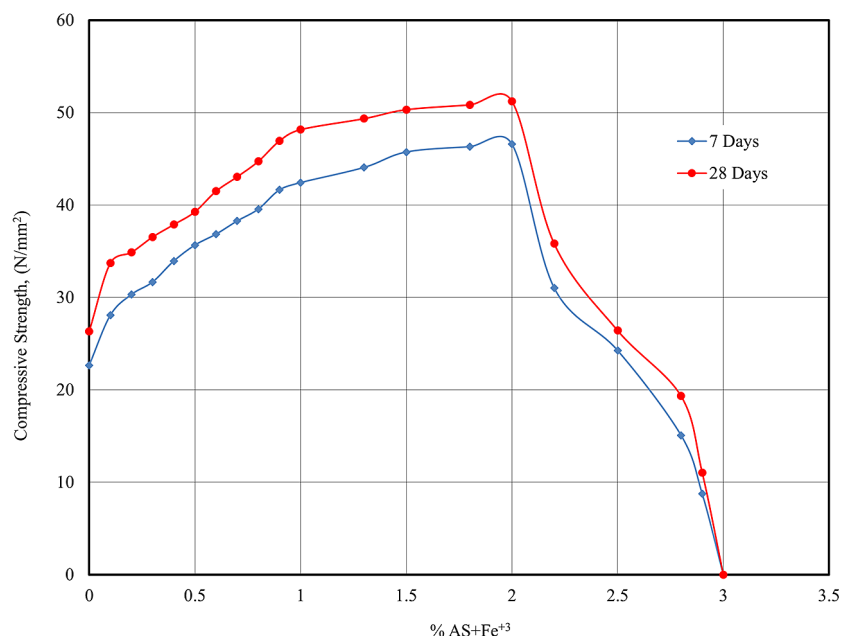


Figure 22. Effect of Fe⁺³-loaded almond shell on the behavior of concrete mixture

element, contributes significantly to the increase in concrete’s compressive strength by penetrating the pores and voids of the concrete mixture, especially when loaded with almond shell. However, when the almond shell ratio exceeds 2, the compressive strength begins to decrease gradually, ultimately leading to the complete failure of the samples at a ratio of 3. This outcome can be attributed to the same factors observed with the addition of almond shell alone.

CONCLUSIONS

Almond shells are discarded as one of the agricultural wastes in large quantities. This study aimed to investigate the optimal utilization of these important agricultural residues in removing iron (III) ions by adsorption technique, as a treatment method for an important and sustainable water source, which is the produced water associated with the production of crude oil produced from the Al-Ahdab oil field in Wasit Governorate, eastern Iraq. The obtained results showed a

good ability of almond shells to recover iron (III) ions from aqueous solutions, with an efficiency of more than 96% at operating conditions of 5, 400 rpm, 85 ppm, 45 g/l, 150 min and 50 °C for each of pH, agitation speed, initial concentration of iron (III) ions, adsorbent dose, contact time and temperature, respectively. The morphological examinations showed that virgin almond shells had a small surface area of 7.7 m²/g according to BET surface area analysis, in addition, having an organized and homogeneous surface according to SEM test and multiple functional groups according to FTIR test. The results also demonstrated that the Langmuir model and the intraparticle diffusion model most accurately describe the adsorption process based on the isothermal and kinetic studies, respectively. Additionally, the thermodynamic analysis revealed that the adsorption is spontaneous, endothermic, characterized by decreasing randomness, and of a chemical nature. Finally, the results of using almond shells loaded with iron showed excellent ability to improve the compressive strength of the concrete mixture prepared in the ratios (4:2:1) of (cement:sand:gravel),

as the compressive strength increased from 34–51 N/mm² approximately for the concrete mixture at the age of 28-days. With these results, the current study concluded that integrated management of agricultural waste can provide a sustainable material for treating polluted water and a sustainable source of water that can be used in various fields, as well as exploiting the residues in preparing a reinforcing material for concrete, leading to the realization of the concept of zero residue level.

Acknowledgments

The authors would like to thank Mustansiriyah University (www.uomustansiriyah.edu.iq), Baghdad – Iraq, and Mutah University (www.mutah.edu.jo/), Al Karak – Jordan, for their support in the present work.

REFERENCES

1. Abbas F.S., Abdulkareem W.S., Abbas M.N. (2022a). Strength development of plain concrete slabs by the sustainability potential of lead-loaded rice husk (LLRH). *Journal of Applied Engineering Science*, 20, 1, 160–167. <https://doi.org/10.5937/jaes0-32253>
2. Abbas M.N. (2015). Phosphorus removal from wastewater using rice husk and subsequent utilization of the waste residue. *Desalination and Water Treatment*, 55, 4, 970–977. <https://doi.org/10.1080/19443994.2014.922494>
3. Abbas M.N., Abbas F.S. (2013a). Iraqi rice husk potency to eliminate toxic metals from aqueous solutions and utilization from process residues. *Advances in Environmental Biology*, 7(2), 308–319. <https://www.aensiweb.com/old/aeb/2013/308-319.pdf>
4. Abbas M.N., Abbas F.S. (2013b). The predisposition of iraqi rice husk to remove heavy metals from aqueous solutions and capitalized from waste residue. *Research Journal of Applied Sciences, Engineering and Technology*, 6, 22, 4237–4246. <https://www.maxwellsci.com/html/rjaset.6.3539.html>
5. Abbas M.N., Abbas F.S. (2013c). the feasibility of rice husk to remove minerals from water by adsorption and avail from wastes. *Research Journal of Applied Sciences, WSEAS Transactions on Environment and Development*, 9(4), 301–313. <http://www.wseas.org/multimedia/journals/environment/2013/145715-140.pdf>
6. Abbas M.N., Abbas F.S. (2014). Application of rice husk to remove humic acid from aqueous solutions and profiting from waste leftover. *WSEAS Transactions on Biology and Biomedicine*, 11(9), 62–69. <http://www.wseas.us/journal/pdf/biology/2014/a025708-124.pdf>
7. Abbas M.N., Alalwan H.A. (2019). Catalytic oxidative and adsorptive desulfurization of heavy naphtha fraction. *Korean Journal of Chemical Engineering*, 12(2), 283–288. <http://doi.org/10.9713/kcer.2019.57.2.283>
8. Abbas M.N., Ali S.T., Abbas R.S. (2020). Rice husks as a biosorbent agent for Pb⁺² ions from contaminated aqueous solutions: a review. *Biochemical and Cellular Archives*, 20(1), 1813–1820. <https://doi.org/10.35124/bca.2020.20.1.1813>
9. Abbas M.N., Al-Hermizy S.M.M., Abudi Z.N., Ibrahim T.A. (2019a). Phenol biosorption from polluted aqueous solutions by *Ulva lactuca* alga using batch mode unit. *Journal of Ecological Engineering*, 20(6), 225–235. <https://doi.org/10.12911/22998993/109460>
10. Abbas M.N., Al-Madhhachi A.T., Esmael S.A. (2019b). Quantifying soil erodibility parameters due to wastewater chemicals. *International Journal of Hydrology Science and Technology*, 9(5), 550F568. <http://doi.org/10.1504/IJHST.2019.10016884>
11. Abbas M.N., Al-Tameemi I.M., Hasan M.B., Al-Madhhachi A.T. (2021). Chemical removal of cobalt and lithium in contaminated soils using promoted white eggshells with different catalysts. *South African Journal of Chemical Engineering*, 35, 23–32. <https://doi.org/10.1016/j.sajce.2020.11.002>
12. Abbas M.N., Ibrahim S.A. (2020). Catalytic and thermal desulfurization of light naphtha fraction. *Journal of King Saud University - Engineering Sciences*, 32(4), 229–235. <https://doi.org/10.1016/j.jksues.2019.08.001>
13. Abbas M.N., Ibrahim S.A., Abbas Z.N., Ibrahim T.A. 2022b. Eggshells as a Sustainable Source for Acetone Production. *Journal of King Saud University - Engineering Sciences*, 34(6), 381–387. <https://doi.org/10.1016/j.jksues.2021.01.005>
14. Abbas M.N., Nussrat T.H. 2020. Statistical Analysis of Experimental Data for Adsorption Process of Cadmium by Watermelon Rinds in Continuous Packed Bed Column. *International Journal of Innovation, Creativity and Change*, 13(3), 124–138. https://www.ijicc.net/images/vol_13/Iss_3/13321_Abbas_2020_E_R.pdf
15. Abd ali I.K., Ibrahim T.A., Farhan A.D., Abbas M.N. 2018. Study of the effect of pesticide 2,4-D on the histological structure of the lungs in the albino mice (*Mus musculus*). *Journal of Pharmaceutical Sciences and Research*, 10(6), 1418–1421. <https://www.jpsr.pharmainfo.in/Documents/Volumes/vol10Issue06/jpsr10061822.pdf>
16. Abd Ali I.K., Salman S.D., Ibrahim T.A., Abbas M.N. (2024). Study of the Teratogenic Effects of Antimony on Liver in the Adult Rabbit (*Oryctolagus*

- cuniculus*). *Advancements in Life Sciences*, 11(2), 462–469. <http://dx.doi.org/10.62940/als.v11i2.2773>
17. Abd Al-Latif F.S., Ibrahim T.A., Abbas M.N. (2023). Revealing potential histological changes of deltamethrin exposure on testicular tissue in albino rabbits (*Oryctolagus cuniculus*). *Advancements in Life Sciences*, 10(4), 619–626. <http://dx.doi.org/10.62940/als.v10i4.2323>
 18. Abdulkareem W.S., Aljumaily H.S.M., Mushatat H.A., Abbas M.N. (2023). Management of Agro-Waste by Using as an Additive to Concrete and Its Role in Reducing Cost Production: Impact of Compressive Strength as a Case Study. *International Journal on “Technical and Physical Problems of Engineering” (IJTPE)*, 15(1), 62–67. <http://www.iotpe.tabaelm.com/IJTPE/IJTPE-2023/IJTPE-Issue54-Vol15-No1-Mar2023/9-IJTPE-Issue54-Vol15-No1-Mar2023-pp62-67.pdf>
 19. Abdullah W.R., Alhamadani Y.A.J., Abass I.K., Abbas M.N. (2023). Study of chemical and physical parameters affected on purification of water from inorganic contaminants. *Periodicals of Engineering and Natural Sciences*, 11(2), 166–175. <http://dx.doi.org/10.21533/pen.v11i2.3508>
 20. Al-Ali S.I.S., Abudi Z.N., Abbas M.N. (2023). Modelling and simulation for the use of natural waste to purified contaminated heavy metals. *Journal of the Nigerian Society of Physical Sciences*, 5(1), 1143. <https://doi.org/10.46481/jnsps.2023.1143>
 21. Alalwan H.A., Abbas M.N., Abudi Z.N., Alminshid A.H. (2018). Adsorption of thallium ion (Tl^{+3}) from aqueous solutions by rice husk in a fixed-bed column: Experiment and prediction of breakthrough curves. *Environmental Technology and Innovation*, 12, 1–13. <https://doi.org/10.1016/j.eti.2018.07.001>
 22. Alalwan H.A., Abbas M.N., Alminshid A.H. (2020). Uptake of cyanide compounds from aqueous solutions by lemon peel with utilising the residue absorbents as rodenticide. *Indian Chemical Engineer*, 62(1), 40–51. <https://doi.org/10.1080/00194506.2019.1623091>
 23. Alalwan H.A., Mohammed M.M., Sultan A.J., Abbas M.N., Ibrahim T.A., Aljaafari H.A.S., Alminshid A.A. (2021). Adsorption of methyl green stain from aqueous solutions using non-conventional adsorbent media: Isothermal kinetic and thermodynamic studies. *Bioresource Technology Reports*, 14, 100680. <https://doi.org/10.1016/j.biteb.2021.100680>
 24. Alhamd S.J., Abbas M.N., Al-Fatlawy H.J.J., Ibrahim T.A., Abbas Z.N. (2024b). Removal of phenol from oilfield produced water using non-conventional adsorbent medium by an eco-friendly approach. *Karbala International Journal of Modern Science (KIJOMS)*, 10(2), 191–210. <https://doi.org/10.33640/2405-609X.3350>
 25. Alhamd S.J., Abbas M.N., Manteghian M., Ibrahim T.A., Jarmondi K.D.S. (2024a). Treatment of oil refinery wastewater polluted by heavy metal ions via adsorption technique using non-valuable media: cadmium ions and buckthorn leaves as a study case. *Karbala International Journal of Modern Science (KIJOMS)*, 10(1), 1–18. <https://doi.org/10.33640/2405-609X.3334>
 26. Al-Hermizy S.M.M., Al-Ali S.I.S., Abdulwahab I.A., Abbas M.N. (2022). Elimination of zinc ions (Zn^{+2}) from synthetic wastewater using lemon peels. *Asian Journal of Water, Environment and Pollution*, 19(5), 79–85. <https://doi.org/10.3233/AJW220073>
 27. Ali G.A.A., Abbas M.N. (2020). Atomic spectroscopy technique employed to detect the heavy metals from iraqi waterbodies using natural bio-filter (*Eichhornia crassipes*) thera dejla as a case study. *Systematic Reviews in Pharmacy*, 11(9), 264–271. <https://doi.org/10.31838/srp.2020.9.43>
 28. Ali G.A.A., Ibrahim S.A., Abbas M.N. (2021). Catalytic adsorptive of nickel metal from iraqi crude oil using non-conventional catalysts. *Innovative Infrastructure Solutions*, 6(7), 1–9. <https://doi.org/10.1007/s41062-020-00368-x>
 29. Ali S.A.K., Abudi Z.N., Abbas M.N., Alsaffar M.A., Ibrahim T.A. (2024). Synthesis of nano-silica particles using *Eucalyptus globulus* leaf extract and their innovative application as an adsorbent for malachite green dye. *Russian Journal of Applied Chemistry*, 97(1), 2–14. <https://doi.org/10.1134/S1070427224010099>
 30. Ali S.A.K., AL-Kaabi Z., Kasim M.N., Abbas M.N., Ibrahim T.A. (2023). Remediation of antimony from aqueous solutions by adsorption technique: isothermal, kinetic and thermodynamic studies. *Indian Journal of Environmental Protection*, 43(14), 1316–1325, (Conference 2023). <https://www.e-ijep.co.in/43-14-1316-1325/>
 31. Ali S.A.K., Almhana N.M., Hussein A.A., Abbas M.N. (2020a). Purification of aqueous solutions from toxic metals using laboratory batch mode adsorption unit antimony (V) ions as a case study. *Journal of Green Engineering (JGE)*, 10(11), 10662–10680.
 32. Ali S.T., Qadir H.T., Moufak S.K., Al-Badri M.A.M., Abbas M.N. (2020b). a statistical study to determine the factors of vitamin D deficiency in men: the City of Baghdad as a model. *Indian Journal of Forensic Medicine & Toxicology*, 14(1), 691–696. <https://doi.org/10.37506/ijfmt.v14i1.132>
 33. Ali S.T., Shahadha R.W., Abdulkareem W.S., Abbas M.N. (2024). Available low cost agro-waste as an efficient medium to eliminate heavy metal contamination using sustainable approach achieving zero residue level. *Journal of Ecological Engineering*, 25(10), 160–175. <https://doi.org/10.12911/22998993/191945>

34. Alminshid A.H., Abbas M.N., Alalwan H.A., Sultan A.J., Kadhme M.A. (2021). Aldol condensation reaction of acetone on MgO nanoparticles surface: An *in-situ* drift investigation. *Molecular Catalysis*, 501, 111333. <https://doi.org/10.1016/j.mcat.2020.111333>
35. Alsarayreh, A.A., Ibrahim, S.A., Alhamd S.J., Ibrahim T.A., Abbas M.N. (2024). Removal of selenium ions from contaminated aqueous solutions by adsorption using lemon peels as a non-conventional medium. *Karbala International Journal of Modern Science (KIJOMS)*, 10(4), 511–531. <https://doi.org/10.33640/2405-609X.3375>
36. Alwan E.K., Hammoudi A.M., Abd I.K., Abd Alaa M.O., Abbas M.N. (2021). Synthesis of Cobalt Iron Oxide Doped by Chromium Using Sol-Gel Method and Application to Remove Malachite Green Dye. *NeuroQuantology*, 19(8), 32–41 <http://doi:10.14704/nq.2021.19.8.NQ21110>
37. Bakker E.S., Van Donk E., Immers A.K. (2016). Lake restoration by in-lake iron addition: a synopsis of iron impact on aquatic organisms and shallow lake ecosystems. *Aquatic Ecology*, 50, 121–135. <https://doi.org/10.1007/s10452-015-9552-1>
38. Bayuo J., Rwiza M.J., Sillanpää M., Mtei K.M. (2023). Removal of heavy metals from binary and multicomponent adsorption systems using various adsorbents - a systematic review. *RSC advances*, 13(19), 13052–13093. <https://doi.org/10.1039/d3ra01660a>
39. Ejaz U., Khan S.M., Khalid N., Ahmad Z., Jehangir S., Fatima Rizvi Z., Lho L.H., Han H., Raposo A. (2023). Detoxifying the heavy metals: a multipronged study of tolerance strategies against heavy metals toxicity in plants. *Frontiers in plant science*, 14, 1154571. <https://doi.org/10.3389/fpls.2023.1154571>
40. Ghulam N.A., Abbas M.N., and Sachit D.E. (2020). Preparation of synthetic alumina from aluminium foil waste and investigation of its performance in the removal of RG-19 dye from its aqueous solution. *Indian Chemical Engineer*, 62(3), 301–313. <https://doi.org/10.1080/00194506.2019.1677512>
41. Hamdi G.M., Abbas M.N., Ali S.A.K. (2024). Bio-ethanol production from agricultural waste: a review. *Journal of Engineering and Sustainable Development*, 28(2), 233–252. <https://doi.org/10.31272/jeasd.28.2.7>
42. Hameed W.A., and Abbas M.N. (2024). Dyes adsorption from contaminated aqueous solution using SiO₂ nanoparticles prepared from extracted tree leaves. *Journal of Ecological Engineering*, 25(7), 41–57. <https://doi.org/10.12911/22998993/187921>
43. Hasan M.B., Al-Tameemi I.M., Abbas M.N. (2021). Orange peels as a sustainable material for treating water polluted with antimony. *Journal of Ecological Engineering*, 22(2), 25–35. <https://doi.org/10.12911/22998993/130632>
44. Hashem N.S., Ali G.A.A., Jameel H.T., Khurshid A.N., Abbas M.N. (2021). Heavy metals evaluation by atomic spectroscopy for different parts of water hyacinth (*Eichhornia Crassipes*) plants: Banks of Tigris River and Al-Zuhairat Village Sites. *Biochemical and Cellular Archives*, 21(2), 3813–3819. <https://connectjournals.com/03896.2021.21.3813>
45. Ibrahim S.A., Hasan M.B., Al-Tameemi I.M., Ibrahim T.A., Abbas M.N. (2021). Optimization of adsorption unit parameter of hardness remediation from wastewater using low-cost media. *Innovative Infrastructure Solutions*, 6(4), Article number: 200. <https://doi.org/10.1007/s41062-021-00564-3>
46. Ibrahim T.A., Mahdi H.S., Abbas R.S., Abbas, M.N. (2020a). Study the effect of ribavirin drug on the histological structure of the testes in albino mice (*Mus musculus*). *Journal of Global Pharma Technology*, 12(2) Suppl., 142–146. <http://www.jgpt.co.in/index.php/jgpt/article/view/3233>
47. Ibrahim T.A., Mohammed A.M., Abd ali I.K., Abbas M.N., Hussien S.A. (2020b). Teratogenic effect of carbamazepine drug on the histological structure of testes in the albino mouse (*Mus musculus*). *Indian Journal of Forensic Medicine & Toxicology*, 14(4), 1829–1834. <https://doi.org/10.37506/ijfmt.v14i4.11809>
48. Jiménez S., Micó M.M., Arnaldos M., Medina F., Contreras S. (2018). State of the art of produced water treatment. *Chemosphere*, 192, 186–208. <https://doi.org/10.1016/j.chemosphere.2017.10.139>
49. Khaleel L.R., Al-Hermizy, S. M., Abbas, M.N. (2022). Statistical indicators for evaluating the effect of heavy metals on samaraa drug industry water exposed to the sun and freezing. *Tropical Journal of Natural Product Research*, 6(12), 1969–1974. <http://www.doi.org/10.26538/tjnpr/v6i12.12>
50. Khudair S.Y., Alsarayreh, A.A., Abbas M.N. (2024). Adsorption of vanadium from Iraqi crude oil on nano zeolite and alum sludge. *Journal of Engineering and Sustainable Development (JESD)*, 28(6), 762–769. <https://doi.org/10.31272/jeasd.28.6.9>
51. Maddodi S.A., Alalwan H.A., Alminshid A.H., Abbas M.N. (2020). Isotherm and computational fluid dynamics analysis of nickel ion adsorption from aqueous solution using activated carbon. *South African Journal of Chemical Engineering*, 32, 5–12. <https://doi.org/10.1016/j.sajce.2020.01.002>
52. Nguyen M, Tadi P. (2024). Iron Supplementation. Treasure Island (FL): StatPearls. Available from: <https://www.ncbi.nlm.nih.gov/books/NBK557376/>
53. Ning X., Lin M., Huang G., Mao J., Gao Z., Wang X. (2023). Research progress on iron absorption, transport, and molecular regulation strategy in plants. *Frontiers in plant science*, 14, 1190768. <https://doi.org/10.3389/fpls.2023.1190768>

54. Porter J.L., Rawla P. 2024. Hemochromatosis. Treasure Island (FL): StatPearls. Available from: <https://www.ncbi.nlm.nih.gov/books/NBK430862/>
55. Rajaa N., Kadhim F.J., Abbas M.N., Banyhusan Q.S. (2023). The improvement of concrete strength through the addition of sustainable materials (agro-waste loaded with copper ions). 3rd International Conference for Civil Engineering Science (ICCES 2023), *IOP Conf. Series: Earth and Environmental Science*, 1232, 012038, 9. <http://doi.org/10.1088/1755-1315/1232/1/012038>
56. Rajbongshi A., Gogoi S.B. (2024). A review on oilfield produced water and its treatment technologies. *Petroleum Research*. <https://doi.org/10.1016/j.ptlrs.2024.06.003>
57. Shadhan Z.J., Alhamd S., Abbas M.N. (2024). Recovery of vanadium element from wastewater of petroleum refineries using effective adsorbent: Mathematical approach via isothermal, kinetics and thermodynamic simulation. *Al-Qadisiyah Journal for Engineering Sciences (QJES)*, 17(3), 211–219. <https://doi.org/10.30772/qjes.2024.145441.1069>
58. Ukhurebor K.E., Hossain I., Pal K., Jokthan G., Osang F., Ebrima F. and Katal D. (2024). Applications and Contemporary Issues with Adsorption for Water Monitoring and Remediation: A Facile Review. *Topics in Catalysis*, 67, 140–155. <https://doi.org/10.1007/s11244-023-01817-4>
59. Zhang P., Yang M., Lan J., Huang Y., Zhang J., Huang S., Yang Y., Ru J. (2023). Water quality degradation due to heavy metal contamination: health impacts and eco-friendly approaches for heavy metal remediation. *Toxics*, 11(10), 828. <https://doi.org/10.3390/toxics11100828>